Determination of the ν_μ-spectrum of the CNGS neutrino beam by studying muon events in the OPERA experiment

Diplomarbeit

der Philosophisch-naturwissenschaftlichen Fakultät

der Universität Bern

vorgelegt von

Claudia Borer

2008

Leiter der Arbeit:

Prof. Dr. Urs Moser
Laboratorium für Hochenergiephysik

Contents

Introduction

The Standard Model (SM) of particles and interactions successfully describes particle physics. In the last years growing evidence has been established, indicating that the SM must be extended to possibly include new physics. The main indication for such a need has come from neutrino physics. Ten years ago physicists measured for the first time some peculiar properties of neutrinos coming from the atmosphere, using sensitive underground detectors. Compared to the expectation there was a huge amount of neutrinos missing. Three years later another experiment showed a clear deficit of neutrinos, and this time the neutrinos came from the Sun. These observations were then confirmed by experiments based on neutrino beams from particle accelerators, hence proving the disappearance of neutrinos of specific flavours during their travel from the source to the detector and under specific kinematical conditions. The most promising explanation for this is the oscillation of a neutrino type into another to which the detector is not sensitive. The oscillation mechanism of one particle into another is only possible if they possess mass - and the neutrinos are assumed massless according to the SM. So the hypothesis of neutrino oscillation lies beyond the SM.

The OPERA experiment (Oscillation Project with Emulsion tRacking Apparatus) is a neutrino oscillation project with a long baseline travel for the neutrinos, such to be sensitive to the signal of oscillation of atmospheric neutrinos. It is an appearance experiment, the first aiming to directly reveal the oscillation of muon neutrinos into tau neutrinos, $\nu_\mu \rightarrow \nu_\tau$. Muon neutrinos are produced artificially and are sent by means of a high energy neutrino beam from CERN in Geneva to the Gran Sasso Laboratory in Italy (CNGS) over a distance of 732 km. In order to observe ν_τ interactions, the OPERA apparatus consists of electronic detectors and a huge target mass of $1.8kton$ made of lead and nuclear emulsion films, recording these interactions.

Concerning the atmospheric sector of neutrino oscillation, the ν_τ appearance is still an outstanding missing piece of the neutrino oscillation puzzle. The OPERA detector was especially designed to study this subject. Its expected performance can be estimated also thanks to a detailed knowledge of the CNGS neutrino flux. So far, the best knowledge about the CNGS beam only relied on simulations. Since the understanding of the neutrino flux is one of the main ingredients of any oscillation analysis, we have started a study of the CNGS beam flux by using real neutrino interactions collected by OPERA in a first run held in 2007.

The electronic detectors of the experiment, in fact, provide us valuable information about the neutrino interactions. From data collected during the run of autumn 2007, we selected events coming from muon neutrino charged current interactions which produced a muon detected in the electronic detectors of the apparatus. These events are used together with simulated events in an unfolding procedure that allows to infer the original neutrino beam spectrum from the knowledge of the kinematical distribution of the selected muons. The result obtained by the candidate in this Diploma Thesis is a first attempt for such a measurement and will bring to interesting developments towards a deeper understanding of the OPERA neutrino beam.

Chapter 1

Neutrino Physics

1.1 History of the Neutrino

If we look back for more than a hundred years, the knowledge about particles was rather small. That was the time when the research in this field was just at its beginning. It all started with Thomson discovering the electron in the year 1897. Together with the discovery of the radioactivity appeared the β-decay-problem. The radioactive nucleus emits an electron. This is a two-body decay and the energy and momentum of the initial and final state must be conserved. But as measuements showed, this is not at all the case. The energy spectrum of a β-decay electron is continuous. This fact led to Pauli's hypothesis of the neutrino in 1930 [1]: Pauli tried to save the energy conservation principle in suggesting that electrical neutral particles exist in the nuclei, which he called *neutrons*. These particles are of spin $\frac{1}{2}$ and therefore obey the exclusion principle. Pauli also suggested that the *neutrons* are of around the same mass as the electrons [2]. It was Fermi who - in his theory of beta decay (1934) - first referred to these particles as *neutrinos*. But it would last another 20 years until the existence of the neutrinos would be proven experimentally. This happened in the famous experiment by Reines and Cowan in 1956. They measured the cross-section for the inverse β-decay reaction: $p + \overline{\nu}_e \rightarrow n + e^+$ [3].
One year later Pontecorvo enunciated the following assumptions:

- The neutrino and the antineutrino emitted in β-processes are different particles.
- There exist interactions with no conservation of the lepton number.

From these he deduced that it is possible for neutrinos in vacuum to transform into antineutrinos and vice versa. For doing so both the neutrino and antineutrino have to be particle mixtures of two neutral Majorana particles[1]. The oscillations were supposed to take place between an active and a sterile neutrino. Therefore Pontecorvo not only stated neutrino oscillations, but also proposed the existence of sterile neutrinos [4].
Shortly after that, in 1962, was an experiment taking place at the Brookhaven AGS[2], whose aim was to observe interactions of high-energy neutrinos with matter. The neutrinos needed for this were produced through the decay of pions: $\pi^+ \rightarrow \mu^+ + \nu_\mu$ and $\pi^- \rightarrow \mu^- + \overline{\nu}_\mu$. The results of this experiment showed that the neutrinos, which were used, produced only muons and no electrons. This fact led to the question if there are two kinds of neutrinos, as the predictions based on the

---

[1] see Chapter 1.3
[2] Alternating Gradient Synchrotron

theory with $\nu_\mu = \nu_e$ were not consistent with the measurement. The absence of the electrons and also the problem with the forbidden decay $\mu^+ \rightarrow e^+ + \gamma$ would be explained by the fact that $\nu_\mu \neq \nu_e$, i.e. that there exist at least two flavours of neutrinos - the ν_μ was discovered [5]. In 1988, Lederman, Schwartz, and Steinberger were honoured with the Nobel Prize for the discovery of the ν_μ [6].
The model for the energy production for stars on the main-sequence, like our sun, states that the main source is fusion, taking place deep inside the star. Four protons are supposed to form an alpha particle. Doing so they emit neutrinos. With their extremely small interaction cross-section, neutrinos are the only way to see into the interior of a star and so to verify directly the hypothesis of the energy generation via nuclear fusion [7]. An experiment with exactly this aim was constructed by Davis *et al.* deep under the earth in a mine of the Homestake Mining Company in the USA. By using the inverse β-process $^{37}Cl + \nu_e \rightarrow\ ^{37}Ar + e^-$, one hoped to observe solar neutrinos. Besides that, the experiment should have provided an upper limit on the flux of extraterrestrial neutrinos [8]. In 1968 a paper was published by Davis *et al.* [9] which hold a very interesting fact: the predicted neutrino flux was $2.0 \pm 1.2 \times 10^{-35} s^{-1}$ per ^{37}Cl atom. However, the experiment provides an upper limit of $0.3 \times 10^{-35} s^{-1}$ per ^{37}Cl atom. This measured limit is around seven times smaller than the prediction. This fact is referred to as the solar ν deficit problem.
A year earlier, Pontecorvo wrote about solar neutrinos in conjunction with neutrino oscillation. He stated that, if the oscillation length is smaller than the radius of the region of the sun in which neutrinos were produced, oscillations would be smeared out and therefore not directly observable. Anyhow, there would be an effect which can be seen on the Earth: the observable solar neutrino flux must be two times smaller than the total neutrino flux [4].
The Gargamelle heavy liquid chamber was a CERN[3] neutrino experiment. The bubble chamber was exposed to neutrino and antineutrino beams, searching for neutral current (NC) events. These had to be compared with the charged current (CC) interactions:

$$\begin{array}{lll} \text{NC:} & \nu_\mu + N \rightarrow \nu_\mu + hadrons, & \overline{\nu}_\mu + N \rightarrow \overline{\nu}_\mu + hadrons \\ \text{CC:} & \nu_\mu + N \rightarrow \mu^- + hadrons, & \overline{\nu}_\mu + N \rightarrow \mu^+ + hadrons \end{array}$$

One has to take into account that there would be other interpretations of the events found during the experiment than the neutral current hypothesis. The experimental evidence for neutral currents found in 1973 was confirmed by scientists at Fermilab shortly after the discovery at CERN [10, 11].

In summer 1975 Perl and others found the following reaction:

$$e^+ + e^- \rightarrow e^\pm + \mu^\mp + missing\ energy$$

For this they had no explanation. The missing energy and as well the missing momentum required two additional particles or even more:

$$e^+ + e^- \rightarrow e^\pm + \mu^\mp + \geq 2\ undetected\ particles$$

These events were found using SLAC-LBL[4] at centre-of-mass energies of 4 GeV [12]. One year later they came up with a simple hypothesis which could explain all the data: these events are evidence of a pair production of heavy leptons. The mass of these leptons has to be within the range of 1.6 to 2.0 GeV. The temporary name of this new particle was U, standing for 'unknown'.

$$e^+ + e^- \rightarrow U^+ + U^-$$

---

[3] Conseil Européen pour la Recherche Nucléaire; Geneva.

[4] Stanford Linear Accelerator Center - Lawrence Berkeley Laboratory

The produced U's were supposed to decay almost immediately. Then the e and μ in the previous reaction are decay products of the U's. They also claimed that the U decays into a charged lepton and at least two undetected particles, which have to be neutrinos for most of the events.

$$\begin{aligned} U^- &\rightarrow \nu_U + e^- + \overline{\nu}_e \\ U^- &\rightarrow \nu_U + \mu^- + \overline{\nu}_\mu \end{aligned}$$

The above reactions are two possible decay modes [13]. In 1977 the U got its present name - the τ lepton. So the observed events undergo the following reaction:

$$e^+ + e^- \rightarrow \tau^+ + \tau^-$$

The positron electron annihilation produces two τ's which almost immediately decay. Taking into account some newer events, Perl *et al.* measured the mass of the τ to be $m_\tau = 1.90 \pm 0.10\ GeV$. For the corresponding neutrino ν_τ, they found an upper limit $m_{\nu_\tau} < 0.6\ GeV$ [14].

In 1995 Perl and Reines received the Nobel Prize for the "discovery of the τ" and the "detection of the neutrino", respectively [6].

On 24 February 1987 one observed optically the supernova SN1987A. Knowing that a supernova is accompanied by a neutrino burst, scientists working at the Kamiokande II detector[5] searched for events caused by the supernova. They actually found eleven electron events suitable for a neutrino burst. These neutrinos were the first detected ones coming from a supernova [15]. At this time all the available neutrino detectors were not capable to registrate the small time difference between the arriving photons and the neutrinos which would have been proof for their mass. For the detection of cosmic neutrinos, Koshiba (Kamiokande) and Davis (Homestake) won the Nobel Prize in 2002[6].

Beginning in the year 1989, several experiments collected data to determine the number of light neutrino types (eg. LEP (Large Electron-Positron Collider) at CERN and SLC (Stanford Linear Collider) in Stanford). Combining these results we get [16]:

$$N_\nu = 2.991 \pm 0.061$$

As there can only be three types of neutrinos, there wont exist any others than ν_e, ν_μ, and ν_τ. In particular, the first direct evidence for the tau neutrino was reported in the year 2000 by the DONUT[6] collaboration [17].

In the following years the deficit of the solar and atmospheric neutrinos was confirmed by several experiments: in 1998 Super-Kamiokande showed evidence for neutrino oscillation of atmospheric neutrinos, while SNO[7] presented the first direct indication of neutrino oscillation of solar neutrinos in 2001.

One compares the two ratios R_{data}=(observed number of μ-events)/(observed number of e-events) and R_{MC}=(expected number of μ-events)/(expected number of e-events) and gets results of around $R(\mu/e) = R_{data}/R_{MC} \approx 0.6$. The explanation for this observation is neutrino oscillation, favouring the channel $\nu_\mu \leftrightarrow \nu_\tau$. Hence the neutrinos are not massless [18, 19, 20].

At the "Neutrino '98" international physics conference hold in Japan, physicists from the Super-Kamiokande Experiment[8] announced that they had found evidence for neutrino oscillation. Presented data suggest that muon neutrinos disappear into tau neutrinos which were not detected by the experiment. This is due to the neutrino oscillation process that can only happen if neutrinos

---

[5] Large underground water detector sited in the Mozumi mine in Kamioka, Japan. It has the capability to detect neutrinos through the scattering reaction $\nu_e + e \rightarrow \nu_e + e$ and through $\overline{\nu}_e + p^+ \rightarrow e^+ + n$.

[6] Direct Observation of NU Tau, a Fermilab experiment, USA.

[7] Sudbury Neutrino Oscillation, USA

[8] successor of the Kamiokande detector

possess mass [21]. The limits for the neutrino masses are listed in Table 1.1. The possible distinctions between neutrino and antineutrino properties are ignored for the muon and tau familiy [22].

mass limit	CL
$m_{\overline{\nu}_e} < 2\ eV$	95%
$m_{\nu_e} < 225\ eV$	95%
$m_{\nu_\mu} < 0.19\ MeV$	90%
$m_{\nu_\tau} < 18.2\ MeV$	95%

Table 1.1: *Neutrino mass limits and their confidence level. [22]*

1.2 The Standard Model of particles and interactions

The knowledge about particles is united in the Standard Model (SM). The SM is a quantum field theory which describes the fundamental particles as well as the fundamental forces and was formulated in the 1970s. It says that all matter is built up by only a small number of particles. These particles obey the Fermi-Dirac statistics and thus are called fermions. They have half-integer spin. The fermions again are split into two groups: the leptons and the quarks.

Leptons (spin=$\frac{1}{2}$)				**Quarks** (spin=$\frac{1}{2}$)			
Flavour		Mass MeV	Electric charge	Flavour		Mass GeV	Electric charge
e	electron	0.511	-1	u	up	0.31	2/3
ν_e	electron neutrino	≤ 0.010	0	d	down	0.31	-1/3
μ	muon	105.66	-1	c	charm	1.6	2/3
ν_μ	muon neutrino	≤ 0.16	0	s	strange	0.50	-1/3
τ	tau	1777	-1	t	top	180	2/3
ν_τ	tau neutrino	≤ 18	0	b	bottom	4.6	-1/3

Table 1.2: *Fermions [1]*

As one can see in Table 1.2, the leptons are grouped into three flavours. Each flavour consists of a charged lepton and of a neutral one called neutrino. The muon and the tau are heavy versions of the electron, but unlike the electron they are not stable and decay into neutrinos, electrons, and other particles. The muon has a mean lifetime of $2.2 \times 10^{-6}s$, and the much shorter one of the tau is $2.9 \times 10^{-13}s$. The leptons are fundamental particles which do not have a substructure and exist as free particles. As quantum numbers they carry the so called lepton number L and, according to their flavour, lepton flavour numbers (L_e, L_μ, L_τ). The leptons have the assigned value +1 whereas the antileptons have -1 (see Table 1.3). These numbers are conserved.

The quarks as well are grouped into three flavours. Unlike the leptons, they carry fractional electric charge. In each group are two particles which differ in one unit of electric charge. The quantum numbers for the up and down quarks are the isospin itself and the third component of the isospin (isospin symmetry). All other quarks have a quantum number according to their name, eg. strangeness S for the s quark (see Table 1.4).

Particle	L	L_e	L_μ	L_τ
e^-	$+1$	$+1$	0	0
ν_e	$+1$	$+1$	0	0
e^+	-1	-1	0	0
$\overline{\nu}_e$	-1	-1	0	0
μ^-	$+1$	0	$+1$	0
ν_μ	$+1$	0	$+1$	0
μ^+	-1	0	-1	0
$\overline{\nu}_\mu$	-1	0	-1	0
τ^-	$+1$	0	0	$+1$
ν_τ	$+1$	0	0	$+1$
τ^+	-1	0	0	-1
$\overline{\nu}_\tau$	-1	0	0	-1

Table 1.3: *Lepton number conservation [1]*

Flavour	I	I_3	S	C	$B^\star$	T	Q/e
u	1/2	1/2	0	0	0	0	$+2/3$
d	1/2	$-1/2$	0	0	0	0	$-1/3$
s	0	0	-1	0	0	0	$-1/3$
c	0	0	0	$+1$	0	0	$+2/3$
b	0	0	0	0	-1	0	$-1/3$
t	0	0	0	0	0	$+1$	$+2/3$

Table 1.4: *Quark quantum numbers [1]*

Then again each flavour of the quarks occurs in three colours (red, blue, green). Colour is just another quantum number which allows us to distinguish between the single quarks. The strong forces between the quarks cause an effect called quark confinement. Two or three quarks stick together to form particles with net colour zero. Within this particle the quarks behave as they were free. As soon as the distance between them grows, the strong forces increase as well. So quarks cannot be found individually but only in combinations. The particles formed out of three quarks are called baryons (qqq), the one made out of two quarks are the mesons ($q\overline{q}$). The baryons have half-integer spin, whereas the mesons have integer spin. All particles built with quarks belong to the group of hadrons. For some examples see Table 1.5.

Baryons					**Mesons**				
Particle		Quarks	Mass MeV	Spin	Particle		Quarks	Mass MeV	Spin
p^+	proton	uud	938	1/2	π^+	pion	$u\overline{d}$	140	0
n^0	neutron	udd	940	1/2	K^+	kaon	$u\overline{s}$	494	0
Λ^0	lambda	uds	1116	1/2	ρ^-	rho	$d\overline{u}$	776	1
Ω^-	omega	sss	1672	3/2	η_c^0	eta-c	$c\overline{c}$	2980	0

Table 1.5: *Some Hadrons [23]*

The baryon number B is the conserved quantum number of the baryons. The baryon number is the same for all quarks: $B = \frac{1}{3}$. We then get the following relation between electric charge Q, third component of isospin I_3, and baryon number B:

$$\frac{Q}{e} = I_3 + \frac{1}{2}(B + C + S + B^\star + T) \tag{1.1}$$

As mentioned before, the Standard Model not only describes the particles but also their interactions. Two fermions interact with each other exchanging a particle. This particle belongs to the group of bosons which have integral spin and obey the Bose-Einstein statistics. There are four types of interactions:

- **Strong**
  The boson belonging to the strong interaction is the massless gluon. It acts on the colour charge and causes the binding of the quarks inside a particle as well as the neutrons and protons within nuclei.
- **Electromagnetic**
  The particles participating in this interaction are the electrically charged ones. The exchanged boson is the massless photon, acting on the electric charge. Among others, this interaction is responsible for the binding of the electron to the nucleus, forming atoms.
- **Weak**
  The weak interaction has three bosons, the W^+, W^-, and the Z^0. The first two are responsible for charged currents while the Z^0 is for the neutral currents. So the particles experiencing weak interaction are the quarks and the leptons. In comparison to the interactions mentioned above, these bosons not only own mass but are quite heavy particles: $M_W = 80.2GeV$ and $M_Z = 91.2GeV$. They act on the flavour or weak charge.
- **Gravitational**
  The gravitation acts on the mass and therefore on all particles. The corresponding boson is supposed to be the graviton with spin 2, although it is so far not detected. This interaction is the weakest of all and is not included in the SM.

For a good overview see Table 1.6 [1].

Interaction	Mediator	relative range	mass GeV	source	particles experiencing	typical lifetime
strong	gluon g	1	0	colour charge	quarks, gluons	$10^{-23}s$
electromagnetic	photon γ	10^{-2}	0	electric charge	electrically charged	$10^{-20}s$
weak	$W^\pm$ Z^0	10^{-7}	80.2 91.2	flavour (weak charge)	quarks, leptons	$10^{-10}s$
gravity	graviton G	10^{-39}	0	mass	all	-

Table 1.6: *Interactions (Gravity added just for completeness.) [1]*

The SM includes the weak, electromagnetic, and strong force, as well as local symmetries. Thus it is based on the gauge group $SU(3)_C \times SU(2)_L \times U(1)_Y$[9]. As we are interested in the neutrinos, we now concentrate on the weak force. So we do not need the $SU(3)_C$ group describing the strong force [24].

Before sorting our particles into these groups, we need to discuss another property of the fermions, that is, the helicity and handedness, also known as chirality. Helicity is the projection of the intrinsic spin onto the momentum vector:

$$H = \frac{\mathbf{s} \cdot \mathbf{p}}{|\mathbf{s}| \cdot |\mathbf{p}|} = \pm 1 \tag{1.2}$$

The two possible values (±1) represent the two helicity states, which are right helicity (spin parallel to the direction of motion, $H = +1$) and left helicity (spin antiparallel to the direction of motion, $H = -1$). According to this the helicity state depends on the reference frame of which one is looking at the particle. A massive particle now cannot have a definite helicity state as it is possible to find a

---

[9] Y is the hypercharge.

system where one overtakes the particle which therefore changes helicity. So only massless particles own a definite helicity state, as they go with the speed of light.

Handedness on the other hand is an intrinsic quantum number. It describes the states of the spin in a relativistical invariant way. As for helicity there are two handedness states - left L and right R. These states are independent of the reference frame, but they can change while travelling through space without changing helicity.

Now for a particle, e.g. the electron, exist two helicity and two handedness states. The same is true for the antiparticle. Each handedness state can be expressed through a linear combination of helicity states, as the lines in Figure 1.1 show. We also see that for massless particles the helicity is the same as handedness. To describe the properties of the weak force one better uses the handedness, as it is relativistically invariant.

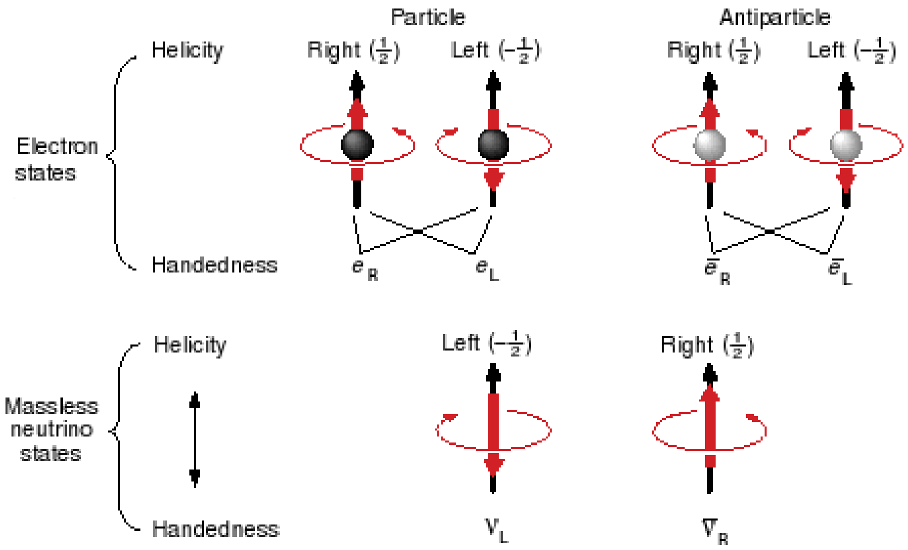

Figure 1.1: *The black arrow represents the momentum, the red one the spin. The lines show that handedness is a linear combination of helicity states. For massless particles handedness is the same as helicity. [25]*

The weak force is left-handed, meaning that it acts on left-handed particles and right-handed antiparticles. The particle states are arranged in weak isospin doublets and singlets. The left-handed electron and electron-neutrino form a weak isospin doublet. Whereas the right-handed electron indeed exists, it is not interacting weakly. Therefore it is a weak isospin singlet. For the antiparticles the same is true, although with opposite handedness. For an overview see Table 1.7 [25].

Handedness	doublets	handedness	singlets
L L	$\begin{pmatrix} e_L \\ \nu_L \end{pmatrix}$	R L	e_R ν_R
R R	$\begin{pmatrix} \bar{e}_R \\ \bar{\nu}_R \end{pmatrix}$	R L	$\bar{e}_L$ $\bar{\nu}_L$

Table 1.7: *Weak isospin doublets. The RH neutrino and the LH antineutrino are not included in the SM. [25]*

To detect neutrinos one needs nucleons and nuclei with which they can react weakly. There are two reactions they can undergo, that is the charged current, CC, and the neutral current, NC.
In the charged current weak interaction, neutrinos react with nucleons which are at rest. So the two possible reactions of a neutrino of flavour l look as follows:

$$\nu_l + n \rightarrow p + l^- \tag{1.3}$$
$$\overline{\nu}_l + p \rightarrow n + l^+ \tag{1.4}$$

These are quasi-elastic reactions, where l stands for e, μ, and τ. For nuclei it looks the same:

$$\nu_l + (Z, A) \rightarrow (Z+1, A) + l^- \tag{1.5}$$
$$\overline{\nu}_l + (Z, A) \rightarrow (Z-1, A) + l^+ \tag{1.6}$$

These reactions depend on the mass of the final lepton, m_l, as well as on the difference of the masses of the nuclear target (e.g. $m_n - m_p = 1.294\ MeV$). These masses make up a threshold for the reactions. For example, if we insert the electron antineutrino and the muon antineutrino, respecitvely, in Eq.(1.4), we get

$$E_{T_e} = (0.511 + 1.294)\ MeV = 1.805\ MeV \tag{1.7}$$
$$E_{T_\mu} = (105.658 + 1.294)\ MeV = 106.952\ MeV \tag{1.8}$$

Reactions with nuclei are more complicated as the target nucleons are bound. Also the momentum distribution of nucleons and the possibility that the final nucleus can be in an excited state make these reactions more difficult.
For high energies occur some side effects such as the excitation of the nucleons or nuclei and the production of additional particles, e.g. pions. If the energy is even higher, the reactions are no longer elastic, on the contrary they turn out to be deep inelastic collisions

$$\nu + N \rightarrow l + X \tag{1.9}$$
$$\overline{\nu} + N \rightarrow l + X \tag{1.10}$$

where X is highly excited hadronic matter and N is a nucleon [26].
Neutrino scattering is another example of weak interaction. The scattering of the neutrinos by charged leptons is considered to be pointlike. The CC scattering takes place between the neutrino and its lepton, exchanging a $W^{\pm}$. There is also a NC scattering which takes place between a neutrino and any lepton, exchanging a Z^0 (see Fig.1.2) [1].

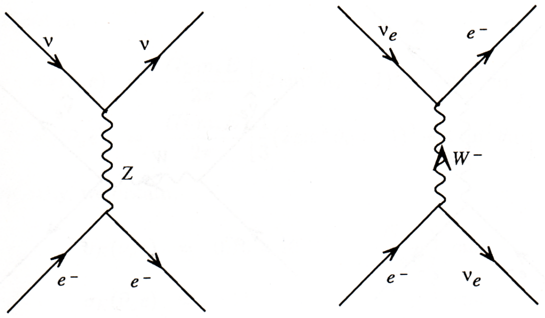

Figure 1.2: *NC and CC neutrino scattering [24]*

Also of great importance are symmetries. There is the parity operation P which inverses spatial coordinates $(x, y, z \rightarrow -x, -y, -z)$. So parity transforms a left-handed system into a right-handed and vice versa. For example let the parity act on the vectors of position and momentum:

$$P(\mathbf{r}) = -\mathbf{r} \tag{1.11}$$

$$P(\mathbf{p}) = -\mathbf{p} \tag{1.12}$$

Parity holds for the strong and electromagnetic interactions, but is violated by the weak force[10]:

$$P|\overline{\nu}_R\rangle \rightarrow \cancel{|\overline{\nu}_L\rangle} \tag{1.13}$$

The left-handed antineutrino does not exist in nature.
Another symmetry is charge conjugation C. As the name already says, it reverses the sign of the charge and the magnetic moment, and changes the sign of all internal quantum numbers (lepton and baryon numbers, strangeness, charm, ...) as well.

$$C(Q) = -Q \tag{1.14}$$

As the electric and magnetic fields are linear in the electric charge, they transform as follows:

$$C(\mathbf{E}) = -\mathbf{E} \tag{1.15}$$

$$C(\mathbf{B}) = -\mathbf{B} \tag{1.16}$$

So the charge conjugation transforms particles into antiparticles:

$$C|\Psi(Q, \mathbf{r}, t)\rangle \rightarrow |\Psi(-Q, \mathbf{r}, t)\rangle \tag{1.17}$$

$$e.g. \quad C|\pi^+\rangle \rightarrow |\pi^-\rangle \tag{1.18}$$

As for the parity, the charge conjugation is invariant for strong and electromagnetic interactions and is violated by the weak force, again shown by the non-existing left-handed antineutrino:

$$C|\nu_L\rangle \rightarrow \cancel{|\overline{\nu}_L\rangle} \tag{1.19}$$

The combination of parity and charge conjugation though is invariant not only for the strong and the electromagnetic interactions but as well for the weak force:

$$CP|\overline{\nu}_R\rangle \rightarrow |\nu_L\rangle \tag{1.20}$$

Both the right-handed antineutrino and the left-handed neutrino exist [28].
There is a third important symmetry operation to take into account, namely the time reversal T. We take a particle collision and reverse all the momenta in direction and all angular momenta. As these quantities are derivatives with respect to time, we would get the same if we just change the sign of the time. This means that two processes with opposite signs in all momenta and angular momenta are invariant under time reversal if they have the same rates [29].

---

[10] Parity was thought to be invariant under all interactions till Madame Wu showed the opposite in an experiment. Using an external magnetic field she forced the spins of ${}^{60}Co$ nuclei at low temperature ($\sim 10mK$) to look in one direction. The β-decay of ${}^{60}Co$ into ${}^{60}Ni$ sends out an electron and an electron-antineutrino:

$${}^{60}Co \rightarrow^{60} Ni + e^- + \overline{\nu}_e$$

Observing the emitted electrons, one found that they preferred the direction opposite to the orientation of the magnetic field. This is only possible if right-handed and left-handed systems are not equivalent. Therefore the weak force violates parity [27].

The combination of all three operations mentioned above leads to the so called CPT theorem, which states that all interactions are invariant under these three operations, independend of the order in which they take place. This theorem results in the properties of particles and antiparticles. Therefore they have the same mass, the same lifetime, and the same electric charges and magnetic moments, although the last two with opposit signs.
It is to mention that CP holds for most weak processes, but not for all. There is CP violation for the neutral kaon K^0. It normally decays into three pions, where CP is conserved. But there is a small probability that the K^0 decays only into two pions, and this process violates CP[11] [1].
Knowing that the CPT theorem holds for all processes, there is only one consequence left: The time reversal invariance is broken for the same processes which violate the CP symmetry [29].

1.3 Beyond the Standard Model

The SM is not complete. We now look at one topic that lies beyond it. As discussed in Chapter 1.1, there is great evidence that neutrinos are not massless. For massive neutrinos exist two concepts, from Dirac and Majorana, concerning particles and antiparticles. The first one states that a Dirac particle is distinct from its antiparticle. If a particle is identical to its antiparticle, then it is a Majorana particle. The difference between a Dirac and Majorana particle depends on the particle's transformation properties, i.e. C, P, T, and its combinations, as well as on the helicity states.
For a better understanding let us take a massive left-handed neutrino, ν_L. We assume CPT to be invariant. Therefore the mirror image of ν_L exists, which is the right-handed antineutrino $\overline{\nu}_R$. If we take into account that our neutrino is massive, hencefort is travelling slower than the speed of light, a frame can be found in which one can overtake the ν_L which then becomes right-handed, ν_R. Assuming that ν_R is not the same as $\overline{\nu}_R$, it then has its own CPT mirror image, $\overline{\nu}_L$. These four states have all the same mass and are called a Dirac neutrino ν^D (see Fig.1.3a).
In the other case, the ν_R from the Lorentz transformation is the same particle as the CPT mirror image of ν_L ($\nu_R \equiv \overline{\nu}_R$). These two states with identical mass form the Majorana neutrino (see Fig.1.3b).

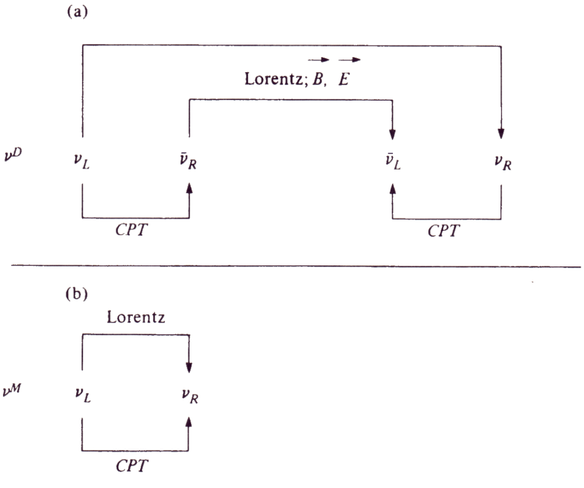

Figure 1.3: *a) The four states of a Dirac neutrino, b) the two states of a Majorana neutrino [26]*

---

[11] for a more detailed description see [1]

It is obvious that the distinction between Majorana and Dirac neutrinos only makes sense for massive neutrinos. Would they actually be massless, one could not overtake a neutrino and therefore helicity could not be changed. So the only two relevant states would be ν_L and $\overline{\nu}_R$, as neutrinos only undergo weak left-handed interactions. The other two states, ν_R and $\overline{\nu}_L$, do not even need to exist. As there are only two relevant states, it does not make sense to distinguish between Dirac and Majorana.
The disappearance of the distinction is actually a continuous process. With decreasing mass/energy it gets more and more difficult to decide to which sort of neutrino the two observed states belong [26].

The neutrinos ν_e, ν_μ, and ν_τ are the so called flavour eigenstates, or the weak states, respectively. These states are superpositions of the mass eigenstates ν_1, ν_2, and ν_3. The weak states propagate through space with different frequencies because of their different masses. After travelling for some distance, they develop different phases. This corresponds to a change in the neutrino flavour, i.e. neutrino oscillation [1].

$$|\nu_\alpha\rangle = \sum_i U_{\alpha i}|\nu_i\rangle \tag{1.21}$$

where $\alpha = e, \mu, \tau$, $i = 1, 2, 3$, and U is the unitary mixing matrix. U is also known as the PMNS (Pontecorvo-Maki-Nakagawa-Sakata) matrix.
If there are only two mass and weak states, the mixing matrix looks as follows (with the mixing angle θ):

$$U = \begin{pmatrix} cos\theta & sin\theta \\ -sin\theta & cos\theta \end{pmatrix} \tag{1.22}$$

whereas for three neutrinos it is:

$$U = \begin{pmatrix} c_{12}c_{13} & s_{12}c_{13} & s_{13}e^{-i\delta} \\ -s_{12}c_{23} - c_{12}s_{23}s_{13}e^{i\delta} & c_{12}c_{23} - s_{12}s_{23}s_{13}e^{i\delta} & s_{23}c_{13} \\ s_{12}s_{23} - c_{12}c_{23}s_{13}e^{i\delta} & -c_{12}s_{23} - s_{12}c_{23}s_{13}e^{i\delta} & c_{23}c_{13} \end{pmatrix} \tag{1.23}$$

with $c_{ij} = cos\theta_{ij}$ and $s_{ij} = sin\theta_{ij}$, the CP violating phase δ, and the three mixing angles θ_{ij} [30]. The PMNS matrix is a rotation. According to present data the neutrino mixing matrix is a rotation with angle $\theta = 56°$. See Fig.1.4 [31].

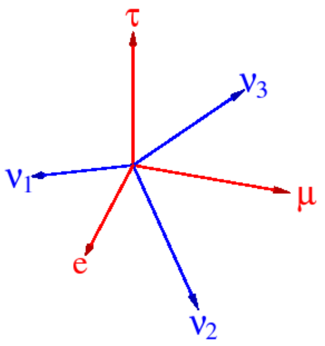

Figure 1.4: *Rotation between mass and weak states. They enclose an angle of $\theta = 56°$. [31].*

1.3.1 Sources for neutrinos

As seen before, atmospheric and solar neutrinos undergo oscillation. Solar neutrinos are produced during nuclear fusion in stars (see Fig.1.5). The flux of solar neutrinos arriving at the Earth is around $7 \times 10^{10}\,\nu\, s^{-1} cm^{-2}$ [32].

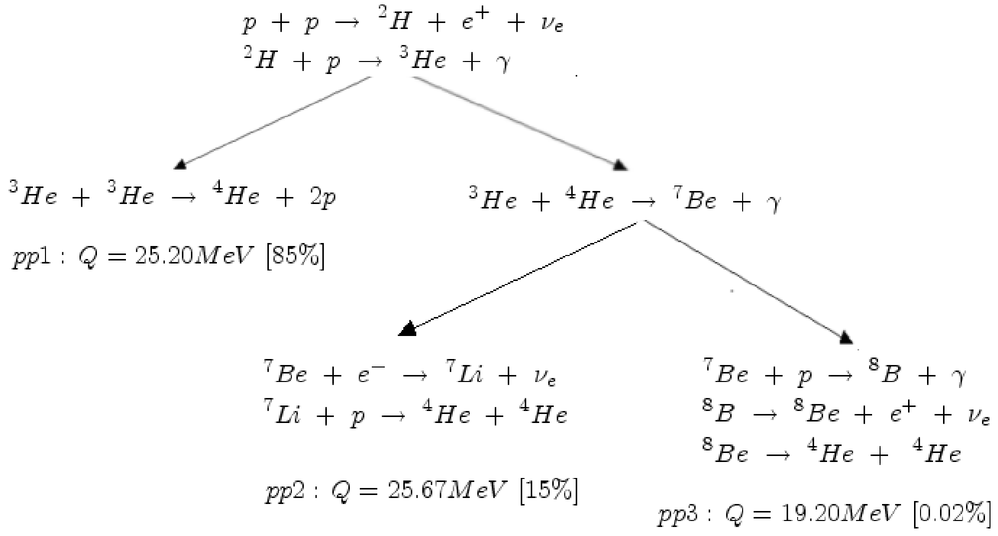

Figure 1.5: *The proton-proton cycle within a star, producing neutrinos. [33]*

The source for atmospheric neutrinos are cosmic rays colliding with nuclei, generating hadronic showers. The ν_e and ν_μ are produced mainly by

$$\pi^+ \rightarrow \mu^+ + \nu_\mu \tag{1.24}$$

$$\pi^- \rightarrow \mu^- + \overline{\nu}_\mu \tag{1.25}$$

$$\mu^+ \rightarrow e^+ + \overline{\nu}_\mu + \nu_e \tag{1.26}$$

$$\mu^- \rightarrow e^- + \nu_\mu + \overline{\nu}_e \tag{1.27}$$

The energy and zenith angle distributions (see Fig.1.6) give direct information for neutrino oscillations, which therefore would solve the atmospheric neutrino problem[12] [34].

Other natural sources for neutrinos are supernovae and the background radiation of the Earth, not discussed further here.

There are neutrinos produced artificially, mainly through nuclear reactors, though nuclear bombs as well generate large amounts of neutrinos. Particle accelerators can be used to produce neutrino beams. For more information see Chapter 2.2, discussing the CNGS beam.

1.3.2 Two flavour neutrino oscillation in vacuum

First we assume that there are only two neutrinos oscillating into each other. Now let us have a look at the neutrino ν_α of Eq.(1.21) and how it evolves in time. For this we apply Schrödinger's equation to ν_i and get

$$|\nu_i(\tau_i)\rangle = e^{-im_i\tau_i}|\nu_i(0)\rangle \tag{1.28}$$

---

[12] see Chaper 1.1

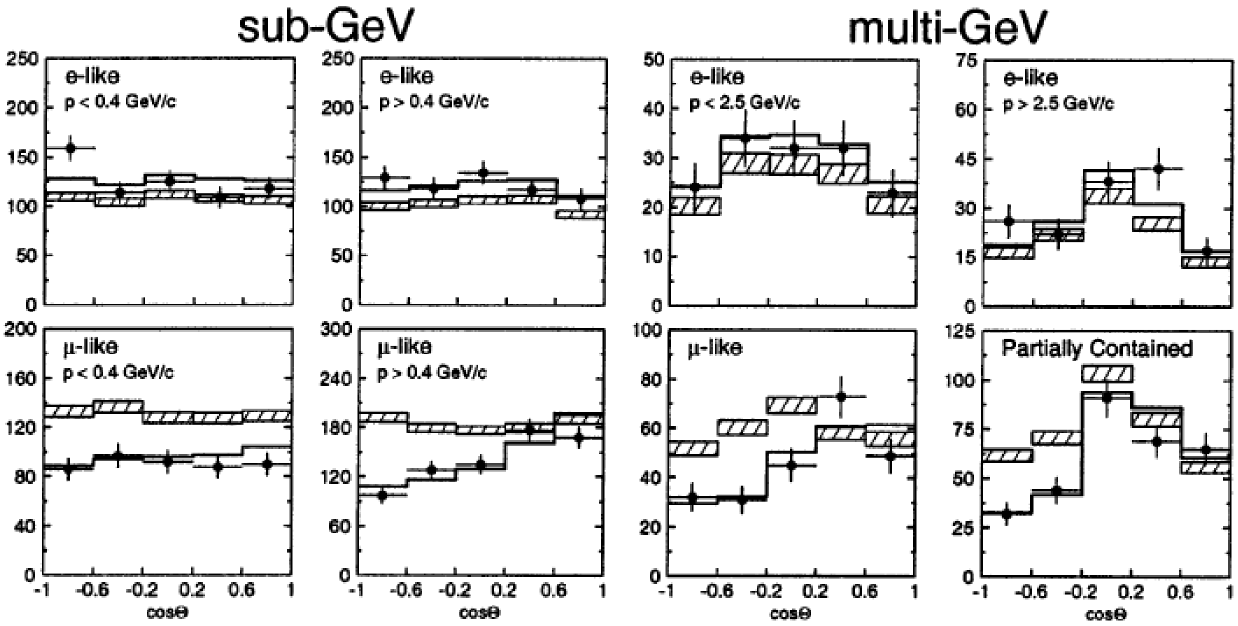

Figure 1.6: *Distribution of the zenith angle for sub-GeV and multi-GeV μ-like and e-like events. The hatched region shows the Monte Carlo expectation if there is no oscillation, where the line shows the expectation for $\nu_\mu \leftrightarrow \nu_\tau$ oscillation [34].*

where m_i is the mass of ν_i, and τ_i is the time (in ν_i's frame). The phase factor in Eq.(1.28) is Lorentz invariant and can be written as

$$e^{-im_i\tau_i} = e^{-i(E_i t - p_i L)} \tag{1.29}$$

where t is the time, L the position, E_i and p_i the energy and momentum of ν_i in the laboratory frame. Our neutrino is extremely relativistic, i.e. we use $t \approx L$ in Eq.(1.29) and get

$$e^{-i(E_i - p_i)L} \tag{1.30}$$

We assume that our ν_α has a definite momentum p, from which follows that all mass eigenstates have the same momentum. Together with the assumption that all the neutrino masses m_i are small compared to p ($m_i \ll p$), this leads to

$$E_i = \sqrt{p^2 + m_i^2} = p\sqrt{1 + \frac{m_i^2}{p^2}} \approx p\left(1 + \frac{1}{2}\frac{m_i^2}{p^2} + \ldots\right) \approx p + \frac{m_i^2}{2p} \tag{1.31}$$

and therefore the phase factor becomes

$$e^{-i\frac{m_i^2}{2p}L} \tag{1.32}$$

The combination of Eq.(1.21) and Eq.(1.32) results in the formula describing the state vector of a neutrino ν_α after the propagation length L:

$$|\nu_\alpha(L)\rangle \approx \sum_i U^\dagger_{\alpha i} e^{-i\frac{m_i^2}{2}\frac{L}{E}} |\nu_i\rangle \tag{1.33}$$

with $E \approx p$ [30]. Out of this we get the probability of a neutrino to change from one flavour into another[13]:

$$P(\nu_\alpha \rightarrow \nu_\beta) = sin^2 2\theta sin^2 \left(1.27\triangle m_{ij}^2\,[eV^2]\,\frac{L\,[km]}{E\,[GeV]}\right) \tag{1.34}$$

with $\alpha \neq \beta$ and $\triangle m_{ij}^2 \equiv |m_i^2 - m_j^2|$ is the mass squared difference. Notice the dependency on L/E. The Super-Kamiokande analysis of atmospheric data limits the value of $\triangle m_{23}^2$ to $2.0 \times 10^{-3} \div 2.7 \times 10^{-3} eV^2$ and $sin^2 2\theta_{23}$ to be greater than 0.93. The most probable solution is $\triangle m_{23}^2 = 2.4 \times 10^{-3} eV^2$ and $sin^2 2\theta_{23} = 1.0$ [35]. The latter is the amplitude in Eq.(1.34). An amplitude of 1.0 means full mixing.

According to Eq.(1.34) the distance a neutrino of flavour α has to traverse in order to be in the same state as in the beginning (α) is the oscillation length L_{osc}[14] [36]:

$$L_{osc}[km] = 2.48 \frac{E\,[GeV]}{\triangle m_{ij}^2\,[eV^2]} \tag{1.35}$$

The oscillation length therefore increases as the mass of the two neutrinos get closer.

So Eq.(1.34) shows that the neutrino flavour oscillates with the distance travelled by the neutrino or with time, respectively. Fig.1.7 shows the time evolution of a muon neutrino produced at the time $t = 0$ as a mixture of the mass eigenstates ν_1 and ν_2.

$$\nu_\mu = -sin\theta\nu_1 + cos\theta\nu_2 \tag{1.36}$$

The frequency of the oscillation of each mass state is determined by its energy. As the two states have different masses, they therefore got also different energies, resulting in different phases.

We get a pure muon neutrino each time the two mass states have the same phases as at the time $t = 0$. At all other times our neutrino is a mixture of the two flavour states ν_μ and ν_e.

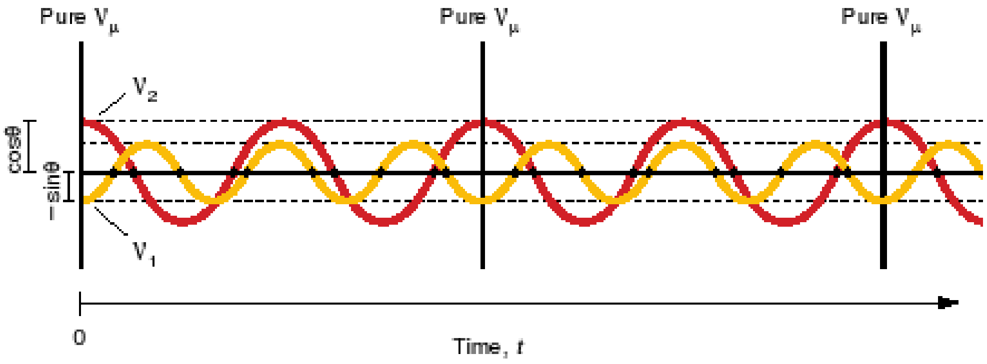

Figure 1.7: *At the time $t = 0$ a muon neutrino was produced. It is a linear mixture of the mass states ν_1 and ν_2: $\nu_\mu = -sin\theta\nu_1 + cos\theta\nu_2$. The phases of the two states evolve in time. If the phases are the same as at $t = 0$, we find a pure muon neutrino, otherwise it is a mixture of the two flavour states ν_μ and ν_e. [25]*

As we assume that there are only two families, the probability of finding a ν_μ and the probability for a ν_e always sum up to 1.

$$P(\nu_\mu \rightarrow \nu_e) + P(\nu_\mu \rightarrow \nu_\mu) = 1 \tag{1.37}$$

In Fig.1.8 we have the purple part representing the probability to find a muon neutrino, where green stands for the probability to find an electron neutrino instead [25].

---

[13] $P(\nu_\alpha \rightarrow \nu_\beta) = |\langle\nu_\beta(0)|\nu_\alpha(L)\rangle|^2$. See Chapter A

[14] see Chapter A

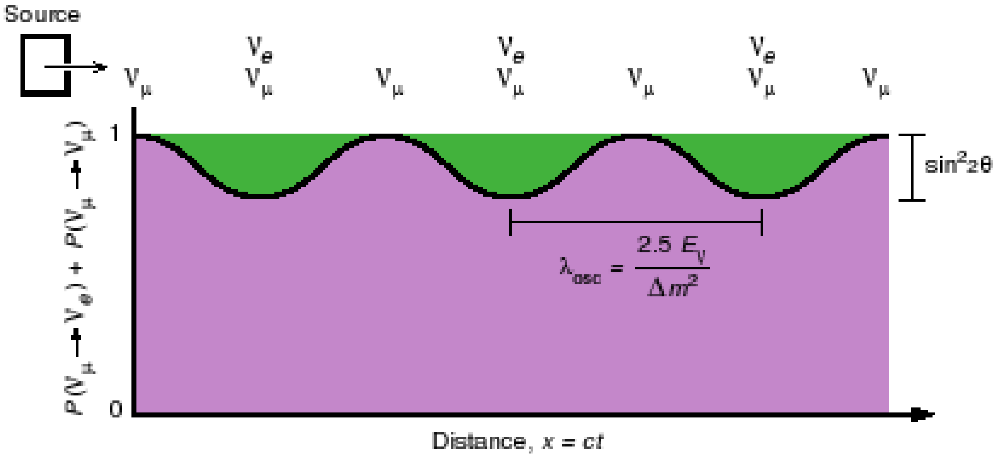

Figure 1.8: *At the beginning is a ν_μ. Purple is the probability of finding a muon neutrino and green the one of finding an electron neutrino. They oscillate with distance and sum up to 1. Indicated are the oscillation length (λ_{osc}) and $sin^2 2\theta$. [25]*

1.3.3 Three flavour neutrino oscillation in vacuum

If there are more than two neutrinos oscillating into each other, the calculation of the probability is more complex. The neutrino mixing in the case of three neutrinos looks as follows:

$$\begin{pmatrix} \nu_1 \\ \nu_2 \\ \nu_3 \end{pmatrix} = U \begin{pmatrix} e^{i\frac{\alpha_1}{2}}\nu_e \\ e^{i\frac{\alpha_2}{2}}\nu_\mu \\ \nu_\tau \end{pmatrix} \tag{1.38}$$

where U is defined in Eq.(1.23) and α_1 and α_2 are two CP violating phases, called Majorana phases. They have no influence on neutrino oscillation per se, whether neutrinos are Majorana particles or not. These two Majorana phases have only physical consequences if neutrinos actually are Majorana particles. If so, these phases have for example an influence on neutrinoless double beta decay[15] [30]. The probability for a neutrino of flavour α to turn in one of flavour β is now

$$\begin{aligned} P(\nu_\alpha \to \nu_\beta) &= \left| \sum_i U_{\alpha i} U^\dagger_{\beta i} e^{-i\frac{m_i^2}{2}\frac{L}{E}} \right|^2 \\ &= \sum_i |U_{\alpha i} U^\dagger_{\beta i}|^2 + \Re \sum_i \sum_{j \neq i} U_{\alpha i} U^\dagger_{\beta i} U^\dagger_{\alpha j} U_{\beta j} e^{i\frac{\triangle m^2_{ij}}{2}\frac{L}{E}} \end{aligned} \tag{1.39}$$

Eq.(1.39) is independent of the Majorana phases, and therefore is identical for Dirac and Majorana particles. As expected, it violates the flavour lepton numbers, though the total lepton number is conserved.

Various experiments on neutrino oscillation were performed providing measurements for the mass squared differences and for the mixing angles. For the actual experimental limits see Table 1.8. Favoured or excluded regions of neutrino parameter space are shown in Fig.1.9.

---

[15] $0\nu\beta\beta$: This is the process $(Z, A) \to (Z + 2, A) + 2e^-$. In this process two neutrinos decay into two protons by emitting two electrons. It violates L conservation and therefore is suppressed. However, there is still a chance to observe it.

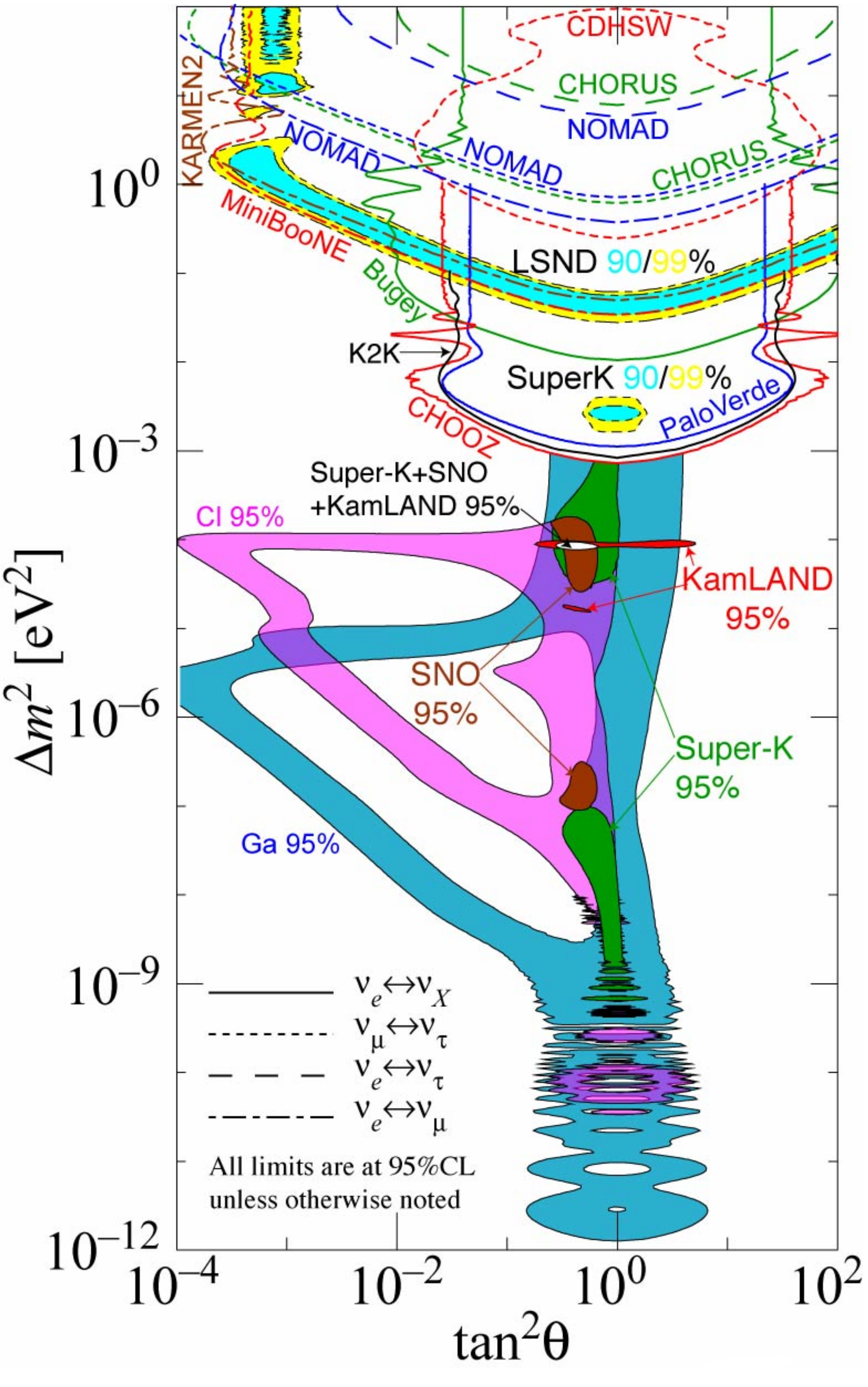

Figure 1.9: *Regions of mass squared difference and mixing angle which are favoured or excluded by various experiments (two neutrino mixing scheme assumed). [37]*

$\triangle m^2_{21} = (8.0^{+0.4}_{-0.3}) \times 10^{-5} eV^2$
$\lvert\triangle m^2_{32}\rvert = (1.9 \div 3.0) \times 10^{-3} eV^2$
$sin^2(2\theta_{12}) = 0.86^{+0.03}_{-0.04}$
$sin^2(2\theta_{23}) > 0.92$
$sin^2(2\theta_{13}) < 0.19$

Table 1.8: *Experimental limits for the neutrino mass squared differences and the mixing angles with* $CL = 90\%$. *At the time being the sign of* $\triangle m^2_{32}$ *is not known. [23]*

The data taken by oscillation experiments is only sensitive to mass squared differences. By convention one associates the mixing angle θ_{12} with solar neutrino oscillations, and m_3 is separated from m_1 and m_2 by a greater interval, $\triangle m^2_{atm}$, than the one between m_1 and m_2, $\triangle m^2_{sol}$. Another assumption is that $m_1 < m_2$. This allows to arrange the mass levels in three different ways [38, 36]:

- **Normal hierarchy**
  In the normal hierarchy the mass m_3 is heavier than the other two: $m_1 \ll m_2 \ll m_3$. In this case the solar neutrino oscillation takes place between the two lighter levels.
- **Inverted hierarchy**
  Opposite to the normal hierarchy the mass m_3 is supposed to be lighter than m_1 and m_2: $m_3 \ll m_1 \simeq m_2$. So the solar neutrino oscillation involves the two heavier levels.
- **Degenerate neutrinos** This is the case if all neutrinos are around the same mass: $m_1 \simeq m_2 \simeq m_3$.

The cases of normal and inverted hierarchy are shown in Fig.1.10. For now we concentrate on atmospheric neutrinos.

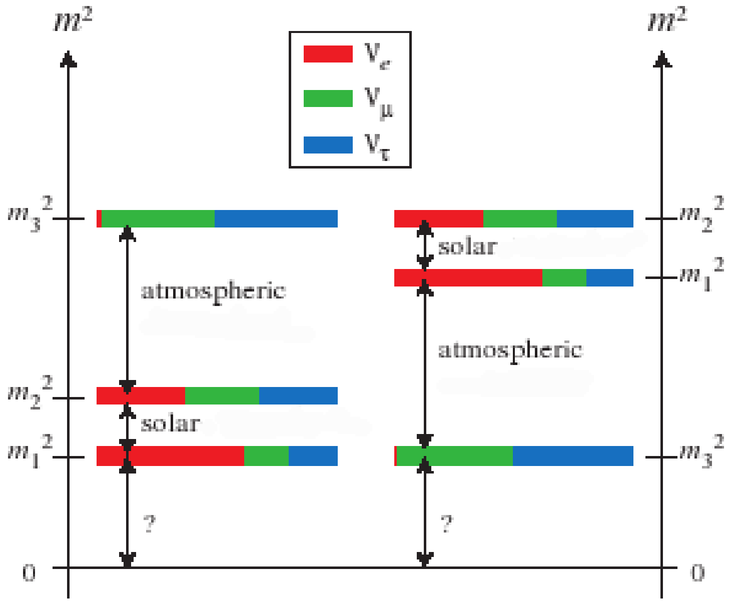

Figure 1.10: *Neutrino mass hierarchy - left: normal hierarchy, right: inverted hierarchy. Indicated is also neutrino mixing. [38]*

We now calculate the probabilities for a muon neutrino to oscillate into a tau neutrino and an electron neutrino, respectively. We can simplify Eq.(1.39) using the fact that $\triangle m^2_{atm} \gg \triangle m^2_{sol}$. This and distances comparable to the atmospheric neutrino oscillation length ($\sim 1000km$) allow us to take only three parameters into account (in zeroth order), i.e. the angles θ_{23} and θ_{13}, as well as $\triangle_{atm} = \triangle m^2_{atm}\frac{L}{4E_\nu}$. One should also consider some first order corrections in $\triangle_{sol} = \triangle m^2_{sol}\frac{L}{4E_\nu}$. Because $sin^2(2\theta_{13})$ is small[16], some terms with $\triangle_{sol}$ are reduced:

$$\begin{aligned}
P(\nu_\mu \to \nu_\tau) &\simeq cos^4(\theta_{13})sin^2(2\theta_{23})sin^2\triangle_{atm} && (1.40)\\
&- \triangle_{sol}cos^2\theta_{13}sin^2(2\theta_{23})(cos^2\theta_{12} - sin^2\theta_{13}sin^2\theta_{12})sin(2\triangle_{atm}) && (1.41)\\
&- \frac{1}{2}\triangle_{sol}cos\delta cos\theta_{13}sin(2\theta_{12})sin(2\theta_{13})sin(2\theta_{23})cos(2\theta_{23})sin(2\triangle_{atm})\\
&+ \triangle_{sol}sin\delta cos\theta_{13}sin(2\theta_{12})sin(2\theta_{13})sin(2\theta_{23})sin^2\triangle_{atm}
\end{aligned}$$

$$\begin{aligned}
P(\nu_\mu \to \nu_e) &\simeq sin^2(2\theta_{13})sin^2(2\theta_{23})sin^2\triangle_{atm}\\
&- triangle_{sol}sin^2\theta_{23}sin^2\theta_{12}sin^2(2\theta_{13})sin(2\triangle_{atm}) && (1.42)\\
&+ \frac{1}{2}\triangle_{sol}cos\delta cos\theta_{13}sin(2\theta_{13})sin(2\theta_{23})sin(2\theta_{12})sin(2\triangle_{atm})\\
&- \triangle_{sol}sin\delta cos\theta_{13}sin(2\theta_{12})sin(2\theta_{13})sin(2\theta_{23})sin^2\triangle_{atm}
\end{aligned}$$

$$P(\nu_\mu \to \nu_\mu) = 1 - P(\nu_\mu \to \nu_e) - P(\nu_\mu \to \nu_\tau)$$

where δ is the CP violating phase of Eq.(1.38) or Eq.(1.23), respectively. The first order corrections in $\triangle_{sol}$ depend on the sign of $\triangle_{atm}$ and hence on the hierarchy [36].

To give an impression for the oscillation lengths, lets have a look at Fig.1.11. What is shown are the oscillation patterns for an initial muon neutrino oscillating into an electron neutrino (black), a muon neutrino (blue), and a tau neutrino (red). In a) one sees nicely the slow solar oscillation. If one zooms in, the solar oscillation becomes negligible and one can observe the fast atmospheric oscillation. The parameters used for these fits are $sin^2\theta_{13} = 0.08$, $sin^2\theta_{23} = 0.95$, $sin^2\theta_{12} = 0.86$, and $\delta = 0$, along with $\triangle m^2_{12} = 8 \times 10^{-5}eV^2$ and $\triangle m^2_{23} \approx \Delta m^2_{13} = 2.4 \times 10^{-3}eV^2$ [39].

1.3.4 Neutrino oscillation in matter

Another important factor to include is matter. As we have seen in Chapter 1.3.2, neutrino oscillation depends on the phase. If the neutrino propagates through matter, the phase will no longer solely depend on the mass state.

All neutrino types interact with quarks and electrons by the exchange of a Z (NC), but only the electron neutrino can interact with electrons by exchanging a W (CC). These two effects have the following corresponding effective potentials:

$$\begin{aligned}
V_{CC}(\nu_e) &= \sqrt{2}G_F N_e\,, \quad V_{CC}(\overline{\nu}_e) = -\sqrt{2}G_F N_e && (1.43)\\
V_{NC}(\nu_e) &= -\frac{1}{\sqrt{2}}G_F N_n && (1.44)
\end{aligned}$$

where N_e is the electron number density and G_F the Fermi constant[17]. There are no analogies for the μ and τ leptons, as they do not exist in normal matter.

---

[16] see Table 1.8

[17] $G_F = 1.16637(1) \times 10^{-5}GeV^{-2}$ [23]

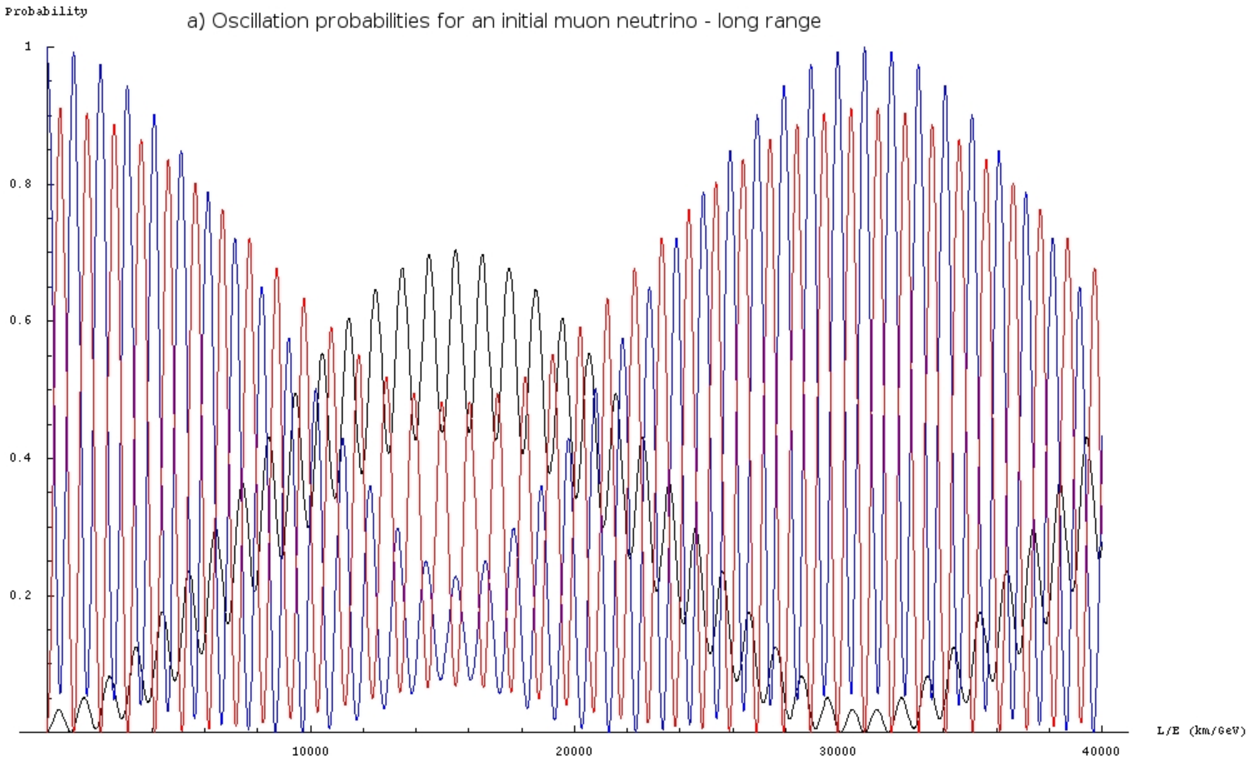

a) Oscillation probabilities for an initial muon neutrino - long range

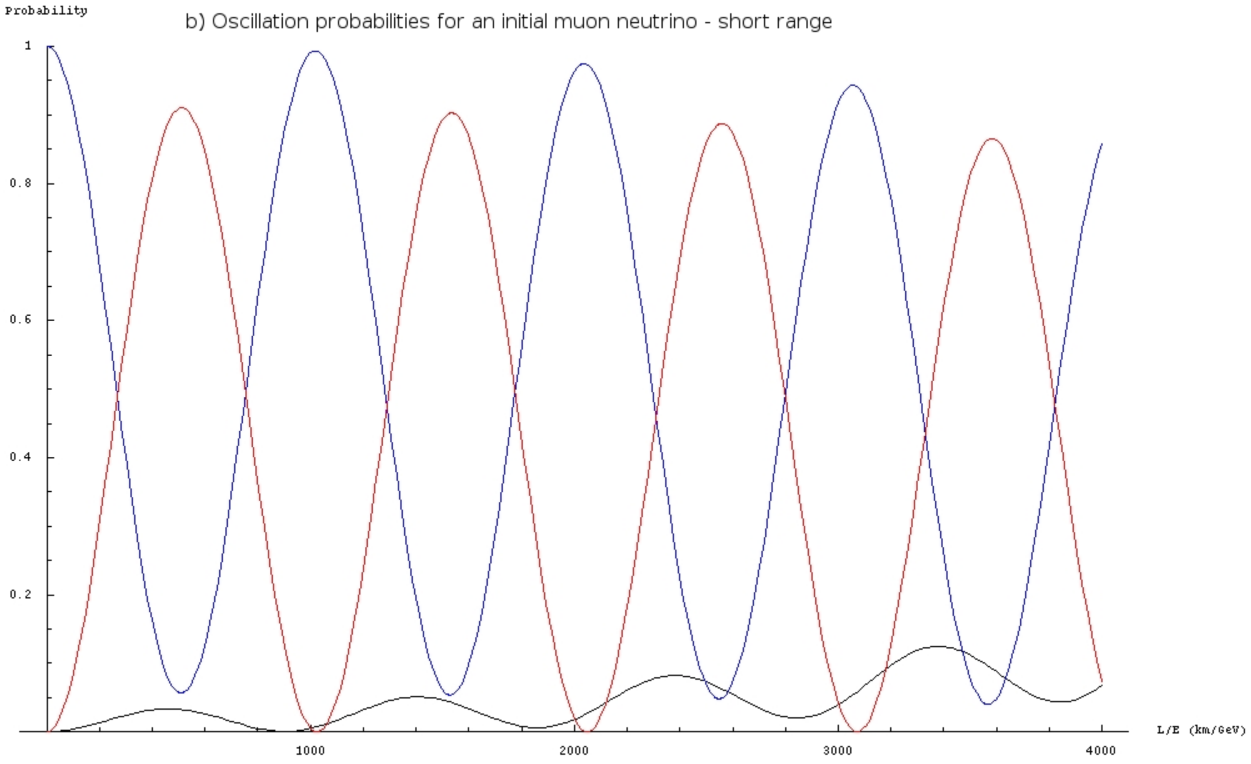

b) Oscillation probabilities for an initial muon neutrino - short range

Figure 1.11: *The probability for an initial muon neutrino to oscillate into a* ν_e *(black), a* ν_τ *(red), and to stay a* ν_μ *(blue). The axis of abscissae shows* L/E *in km/GeV. a) Over a very long range one can observe the slow solar oscillation. This gets negligibly small if one zooms in to observe the fast atmospheric oscillation, b). [39]*

The effective potential causes an additional phase. Therefore we get

$$\nu_e(L) = \nu_e(0)e^{-i\sqrt{2}G_F N_e L} \tag{1.45}$$

for an electron neutrino travelling the distance L through matter, which has a constant density N_e. This leads to the oscillation length in matter:

$$L_0 = \frac{2\pi}{\sqrt{2}G_F N_e} \tag{1.46}$$

In practical units, the effective potential looks like

$$V_{CC} = 7.6\ Y_e\ \frac{\rho}{10^{14}[g/cm^3]}[eV]\,, \quad Y_e = \frac{N_e}{N_p + N_n} \tag{1.47}$$

so the oscillation length becomes

$$L_0 \simeq \frac{1.7 \times 10^7[m]}{\rho[g/cm^3]\ Y_e} \tag{1.48}$$

We compare this result wih the oscillation length obtained in vacuum, Eq.(1.35). As one can see immediately, the main difference is that the oscillation length in matter, L_0, is independent of the neutrino energy.
According to Eq.(1.48), the oscillation length in rock is $L_0 \approx 10^4 km$ and the one in the centre of the Sun is $L_0 \approx 200km$.

We again assume only two mass eigenstates ν_1 and ν_2 and two flavour eigenstates ν_e and ν_α, respectively, together with the oscillation angle θ. The Schrödinger equation then looks like

$$i\frac{d}{dt}\begin{pmatrix} \nu_1 \\ \nu_2 \end{pmatrix} = \begin{pmatrix} \frac{m_1^2}{2E} + V_{CC}c^2 & V_{CC}sc \\ V_{CC}sc & \frac{m_2^2}{2E} + V_{CC}s^2 \end{pmatrix}\begin{pmatrix} \nu_1 \\ \nu_2 \end{pmatrix} \tag{1.49}$$

where $c = cos\theta$ and $s = sin\theta$. We use the following transformation to diagonalise the matrix

$$\nu_{1m} = \nu_e cos\theta_m - \nu_\alpha sin\theta_m \tag{1.50}$$

$$\nu_{2m} = \nu_e sin\theta_m + \nu_\alpha cos\theta_m \tag{1.51}$$

θ_m is the new mixing angle, depending on the vacuum mixing angle θ and on the oscillation lengths L_{osc} (Eq.(1.35)) and L_0 (Eq.(1.48)), respectively:

$$tan2\theta_m = tan2\theta\left(1 - \frac{L_{osc}}{L_0 cos2\theta}\right)^{-1} \tag{1.52}$$

This leads to the effective oscillation length in matter

$$L_m = L_{osc}\frac{sin2\theta_m}{sin2\theta} = L_{osc}\left[1 + \left(\frac{L_{osc}}{L_0}\right)^2 - \frac{2L_{osc}}{L_0}cos2\theta\right]^{-1/2} \tag{1.53}$$

and to the probability to detect a ν_e at a distance L from the ν_e source

$$P(E_\nu, L, \theta, \triangle m^2) = 1 - sin^2 2\theta_m sin^2\frac{\pi L}{L_m} \tag{1.54}$$

It has the usual form, though θ and L_{osc} are replaced by θ_m and L_m [36].

Chapter 2

The OPERA experiment

OPERA stands for **O**scillation **P**roject with **E**mulsion t**R**acking **A**pparatus. It is a long baseline neutrino oscillation project and its goal is to prove that $\nu_\mu \rightarrow \nu_\tau$ is the dominant reaction explaining the oscillation of atmospheric neutrinos. It is an appearance experiment, meaning that it searches for ν_τ appearance in the high energy, almost pure ν_μ CNGS beam[1]. To detect ν_τ interactions one needs a huge target mass with a high resolution. The OPERA detector consists of a $1.8kton$ target made of lead plates and nuclear emulsion films assembled in bricks. The emulsion films provide a high resolution but no time indication. For this we need electronic detectors which we use to reconstruct an event. Their resolution is good enough to locate the brick holding the primary vertex with high probability. A pair of extra emulsion films is attached outside of each brick. Before scanning the whole brick, we have a look at these two emulsions to make sure that we chose the right brick.

The OPERA detector is a hybrid apparatus as it consists of active and passive subdetectors. It is installed in the INFN-LNGS[2] underground laboratory in Gran Sasso, Italy, $732km$ away from the neutrino source located at CERN (see Fig.2.1). So OPERA is optimised to detect muons and taus, but it is also able to study the subdominant $\nu_\mu \rightarrow \nu_e$ oscillation channel [40].

As already mentioned, the distance between CERN and Gran Sasso is $732km$, with an azimuth of $122.5°$ (w.r.t. geographic north) and a slope of -5.6% (w.r.t. the horizontal plane) [41].

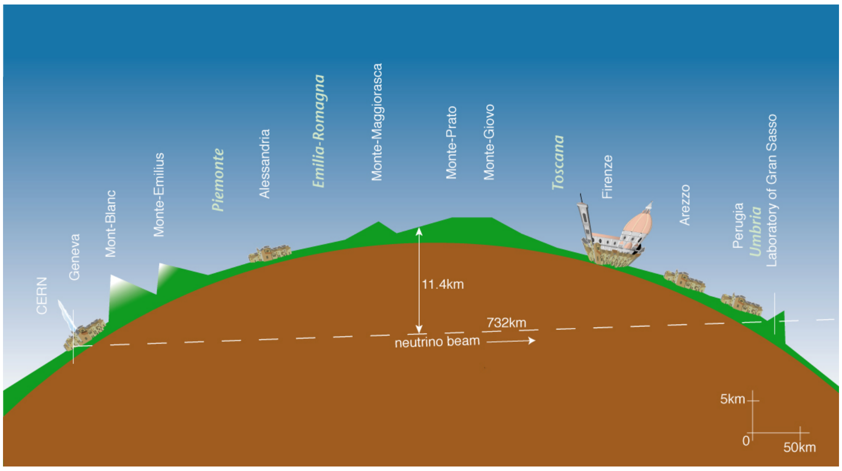

Figure 2.1: *Neutrino beam trajectory [42]*

---

[1] CERN Neutrino Beam to Gran Sasso (see Chapter 2.2)

[2] Istituto Nazionale di Fisica Nucleare - Laboratori Nazionali del Gran Sasso

The L/E ratio of OPERA is

$$\frac{L[km]}{E[GeV]} = \frac{732km}{18.5GeV} \approx 40km/GeV \tag{2.1}$$

If one compares this value with the diagram of Fig.1.11b, one sees that the solar oscillation is negligibly small and that the atmospheric oscillation is still far from its maximum.

2.1 Expected physics performance

OPERA searches for ν_τ appearance by looking for τ^- events generated through CC interactions in the target lead. The mean life time of a τ is $290.6 \times 10^{-15}s$ [23]. It is extremely short-lived and decays almost immediately after its production. The Lorentz boost, however, still allows its detection provided that the detector has very high space resolution ($\lesssim 1mm$ track length). The observable tau decay modes and their branching ratios are listed in Table 2.1. See also Fig.2.2

decay channel	BR
$\tau^- \rightarrow e^-\overline{\nu}_e\nu_\tau$	18%
$\tau^- \rightarrow \mu^-\overline{\nu}_\mu\nu_\tau$	18%
$\tau^- \rightarrow h^-\nu_\tau(n\pi^0)$	50%
$\tau^- \rightarrow 3\pi\nu_\tau(n\pi^0)$	14%

Table 2.1: *τ decay channels observed by OPERA and their branching ratios. [43]*

2.1.1 Signal detection efficiency

As already mentioned, OPERA investigates the e, μ, and hadron as the tau decay channels. They are sorted into two categories, the long and short decays. Short decays only apply for the electron and muon channels. In these cases the tau decays in the same lead plate where the neutrino interaction occurred. The impact parameter of the tau daughter track with respect to the interaction vertex ($IP > 5 \div 20\mu m$) helps selecting tau candidates. On the other hand, the long tau decays apply to all channels. Here the tau is not decaying in the same plate where it was produced and can be reconstructed in one emulsion film. The selection of the tau candidates is due to the existence of a kink angle between the tau and the daughter tracks ($\theta_{kink} > 20mrad$).

One applies a kinematical analysis to the tau candidates found out of the above procedures in order to improve the signal to the background. For short decays the background mainly comes from charm production. Therefore we need a cut on the invariant mass of the hadronic system. It reduces the background immensely.

For long decays one has to consider the leptonic and hadronic decays separately. In the leptonic case one applies a cut on the daughter momentum in order to avoid particle misidentification and to suppress the beam related background. To reduce the background at a reasonable level, one also has to impose a cut on the measured transverse momentum at the decay vertex.

The kinematical analysis is more complicated for the long hadronic decay. The main background comes from the reinteraction of primary hadrons without any visible recoil at the interaction vertex. To keep this background low, one applies cuts at the decay and primary vertex. For the kinematical analysis at the primary vertex one uses the missing transverse momentum at the primary vertex

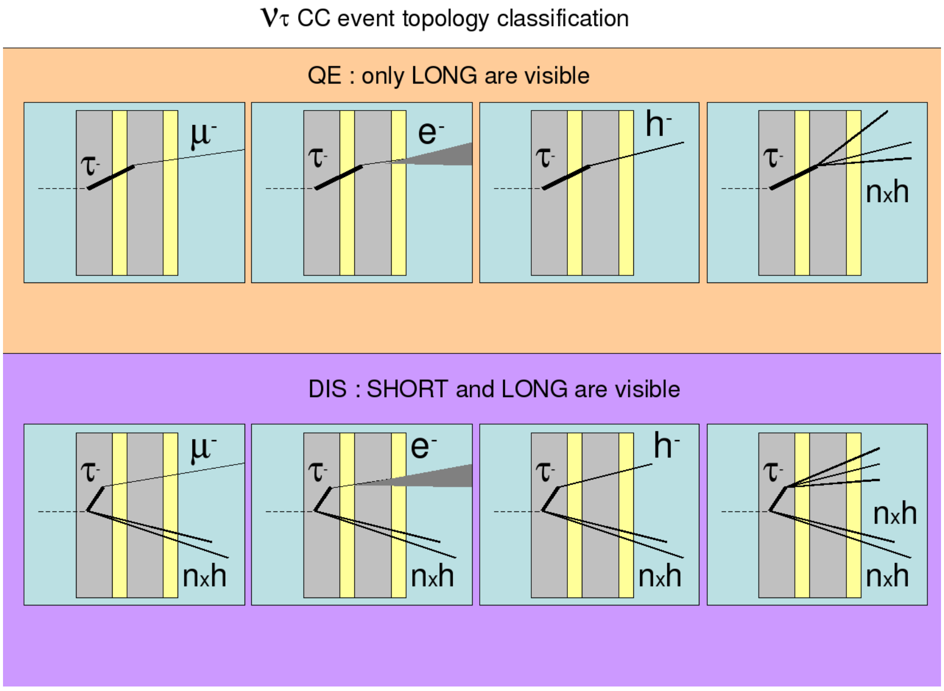

Figure 2.2: *Top: Quasi elastic events. Only long decays visible. Bottom: Deep inelastic events. Both short and long decays visible. Grey symbolises the lead plate, yellow the emulsion film.*

and the angle in the transverse plane between the parent track and the direction of the shower. In NC interactions the missing transverse momentum is supposed to be large due to the unobserved outgoing neutrino. Then again it is expected to be small in CC interactions.
The applied cuts increase the tau detection efficiency at a constant background [40].

2.1.2 Expected background

There are the following main background sources for the observation of a τ coming from the oscillation models:

- Prompt ν_τ production in the primary proton target and in the hadron stopper (see Fig.2.4).
- Background from π^0 and prompt electrons.
- One-prong decay of charmed particles.
- Large angle muon scattering.
- Hadronic reinteractions.

Where the first two backgrounds are very small, the three others likewise contribute to the overall expected background. Fig.2.3 shows a schematic view of the different sources. For now we solely concentrate on the last two.

Large angle muon scattering
In a ν_μ CC event, a muon is produced which then undergoes a scattering in the lead plate directly

following the vertex plate. This can be mistaken as a muonic tau decay. To determine this background experimentally, one measures large angle scattering of $9GeV$ muons in lead plates. For a transverse momentum higher than $250MeV$ and $2mm$ lead, the measured rate is $0.6^{+0.7}_{-0.6} \times 10^{-5}$. Compared with the analytical calculation which predicted a rate of 0.2×10^{-5}, the background was assumed to be of rate 1×10^{-5}.

Hadronic reinteractions

Hadrons produced in ν_μ NC and ν_μ CC events can reinteract without any visible activity at the interaction vertex. Therefore this constitutes an important background source for both the muonic and hadronic channels. If hadronic reinteractions occur in a ν_μ NC event or in a ν_μ CC event with the muon not identified as such, then they are background to the hadronic channel. The expected background rate in the hadronic channel due to hadronic reinteractions is of about 4×10^{-6}. Hadronic reinteractions are background of the muonic channel if either in a ν_μ NC event a hadron is misidentified as a muon or if a muon (identified in the electronic detector) is mismatched to a hadron track in the emulsions. For the muonic channel, there is no kinematical analysis at the primary vertex and p_T is set to be larger than $250MeV$ at the decay vertex. Hence the expected background rate from hadronic reinteractions for the muonic channel is of about 7×10^{-6} [40].

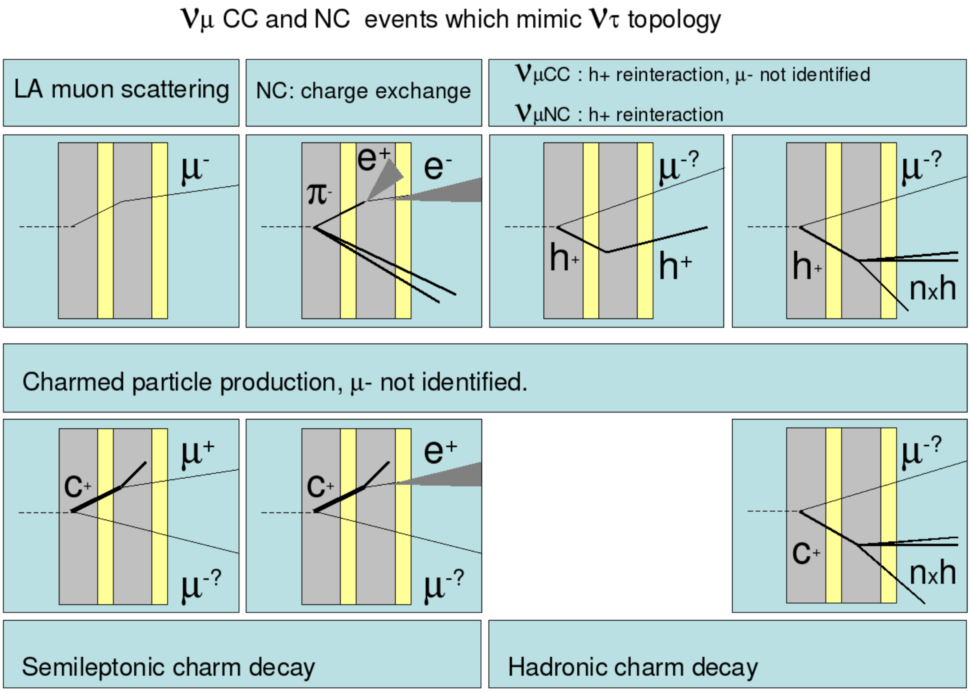

Figure 2.3: *ν_μ interactions mimicing ν_τ events. Grey symbolises the lead plate, yellow the emulsion film.*

2.1.3 Sensitivity to $\nu_\mu \rightarrow \nu_\tau$ oscillations

Now we have a look at the expected τ events and their background. Table 2.2 shows the summarised performance of OPERA after a running time of 5 years with the nominal CNGS beam intensity (status year 2008). For two different values of $\triangle m^2$ at full mixing, which is preferred from atmospheric data (see Chapter 1.3.2), the number of expected signal events from $\nu_\mu \rightarrow \nu_\tau$ is given as a function of the particular decay channels. The main background sources are the decay of charmed

particles, large angle muon scattering, and hadronic reinteractions.
On the basis of the expected background, the probability to detect a given number of events within a 4σ significance leads to the sensitivity of an oscillation experiment.

channel	**signal for** $\triangle m^2 (eV^2)$		**background**
	2.5×10^{-3}	3.0×10^{-3}	
$\tau \rightarrow e$	3.5	5.0	0.17
$\tau \rightarrow \mu$	2.9	4.2	0.17
$\tau \rightarrow h$	3.1	4.4	0.24
$\tau \rightarrow 3h$	0.9	1.3	0.17
Total	10.4	15.0	0.76

Table 2.2: *Summary of expected numbers of tau events in 5 years with nominal CNGS beam intensity*

2.2 The CNGS neutrino beam

The OPERA experiment is based on a ν_μ beam which is as pure as possible. The CNGS neutrino beam was designed and optimised in order to deliver an intense and almost pure ν_μ beam for the study of $\nu_\mu \rightarrow \nu_\tau$ oscillations. $400GeV$ protons get extracted from the CERN SPS in short pulses of $10.5\mu s$ with design intensity of $2.4 \times 10^{13} pot$ (proton on target) per pulse. The protons then hit a graphite target. The target is made out of rods with a diameter of $4mm$ and has a length of $2m$. The protons hitting the target produce secondary pions and kaons of positive charge, which are focussed into a parallel beam via a system of two magnetic coaxial lenses, called horn and reflector. In order to reduce the interaction probability for secondary hadrons, helium bags are placed in the free spaces of the target chamber. A first one between the horn and the reflector, a second one between the reflector and the decay tunnel. This decay tunnel is $1000m$ long and allows the pions and kaons to decay into muon-neutrinos and muons ($\pi : > 99.9\%$; $K : > 63\%$). The long decay tunnel is justified by the decay length of the pion, typically $2.2km$ at $40GeV$. Due to the angular distribution of the parent mesons, the diameter of the tunnel must increase with a longer decay tunnel. For a length of $1000m$ a diameter of $2.45m$ was chosen. At the exit of the decay tunnel was placed a massive iron hadron stopper which absorbs the remaining hadrons (protons, pions, kaons, ...). Downstream of the hadron stopper are two sets of muon spectrometers who monitor the muons and measure their intensity, the beam profile, and its centre. The muons then get absorbed in the rock while the neutrinos continue travelling towards Gran Sasso. For the layout see Fig.2.4.

The CNGS beam intensity is assumed to be $4.5 \times 10^{19} pot/yr$. A run over five years would induce about 31000 CC and NC events. For $sin^2 2\theta_{23} = 1$ and $\triangle m^2_{23} = 2 \times 10^{-3} eV^2$, 95 ν_τ CC interactions out of the 31000 would be expected, respectively 214 ν_τ CC interactions for a $\triangle m^2_{23} = 3 \times 10^{-3} eV^2$. The experiment has already run in 2006-2007 with reduced beam intensity and target mass. The integrated intensity of the autumn 2007 run is $8.24 \times 10^{17} pot$ [44, 45].

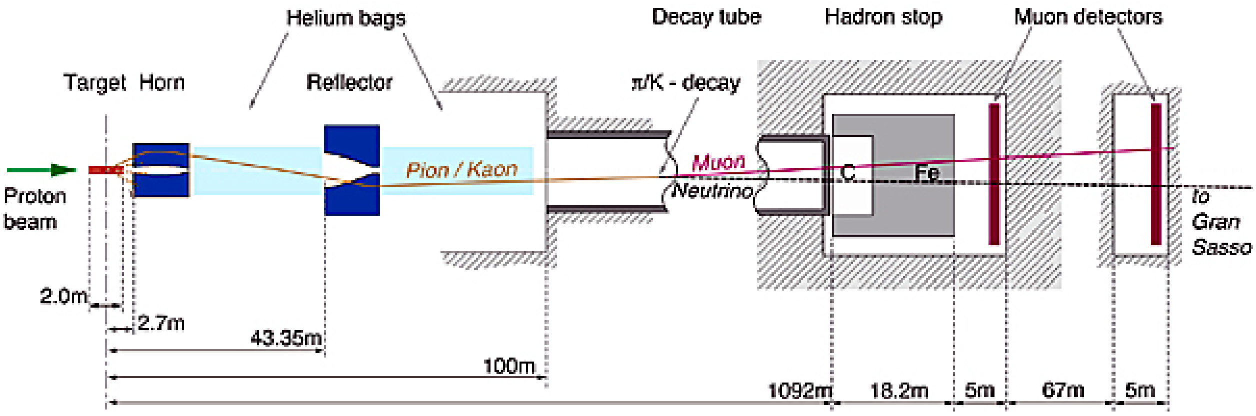

Figure 2.4: *CNGS beam layout. 400GeV protons hit a graphite target producing secondary pions and kaons. The horn and the reflector focus them into a parallel beam. Then they enter the decay tunnel which allows them to decay into μ and ν_μ. All remaining hadrons get absorbed in the hadron stopper. The two muon detectors monitor the muons. Afterwards the muons and neutrinos enter the rock, where the muons get absorbed on the way to Gran Sasso. [42]*

2.3 The OPERA detector

The OPERA detector consists of two identical units, called supermodules. Each one has a target section and a magnetic spectrometer. Additionally a veto system[3] is put in front of the whole detector. The veto has the purpose of tagging interactions occuring in the material upstream of the detector target. Fig.2.5 shows an artistic view of the detector.

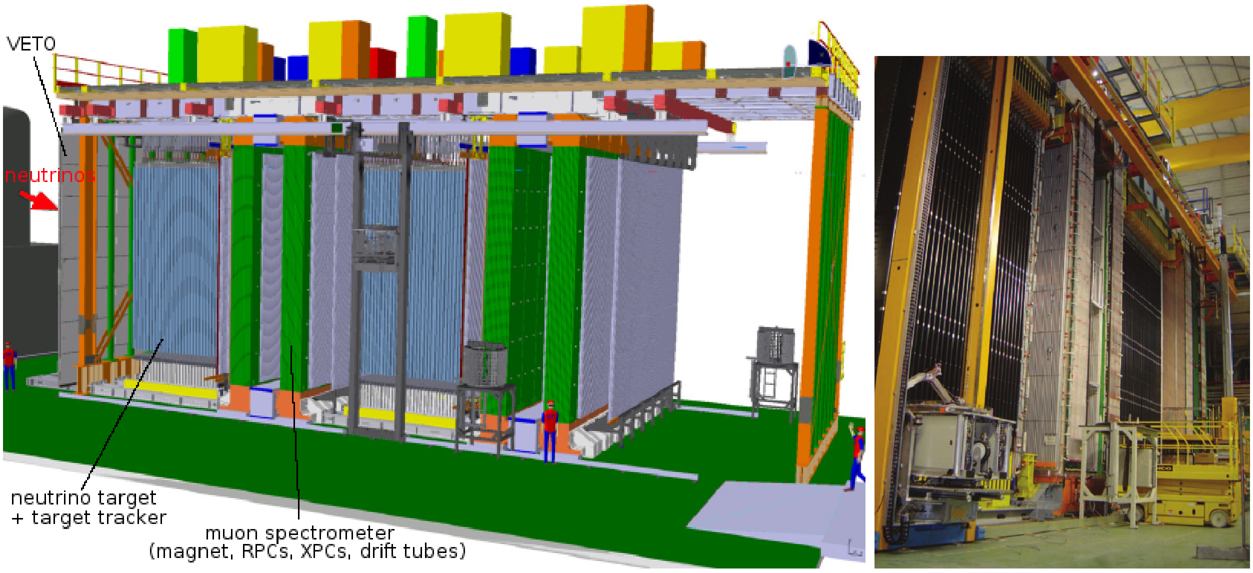

(a)

(b)

Figure 2.5: *a) Artistic view of the OPERA detector, b) photo [44]*

---

[3] see Chapter 2.3.4

2.3.1 Emulsion target

A neutrino experiment needs a huge target mass in order to be able to detect neutrinos. In OPERA we achieve this with an emulsion target containing a large amount of lead. The experiment is based on the Emulsion Cloud Chambers (ECC) technique. This detector is of a modular structure and it is built by alternating plates of a passive material and of nuclear emulsion films. A set of 57 thin emulsion films ($125.10 \times 99.80 \times 0.29 mm^3$) and 56 lead plates ($125.50 \times 100.00 \times 1.00 mm^3$) form a brick (see Fig.2.6). Each emulsion film consists of a $200 \mu m$ thick plastic base which has emulsion layers ($50 \mu m$ thick) on both sides. The emulsion film in front of the first lead plate helps in connecting tracks from the upstream wall. This pile is vacuum wrapped and is called ECC. Its dimension is about $128 \times 103 \times 81 mm^3$ for a total weight of about $8.5 kg$. The thickness corresponds to 10 X_0 which allows to reconstruct electron showers and to measure the momentum by multiple scattering. Additionaly to each brick there are two emulsion films which are attached in a seperate sleeve, called the changeable sheet doublet (CSD). It can be easily detached and analysed, and it is used to confirm tracks in the brick before opening it.

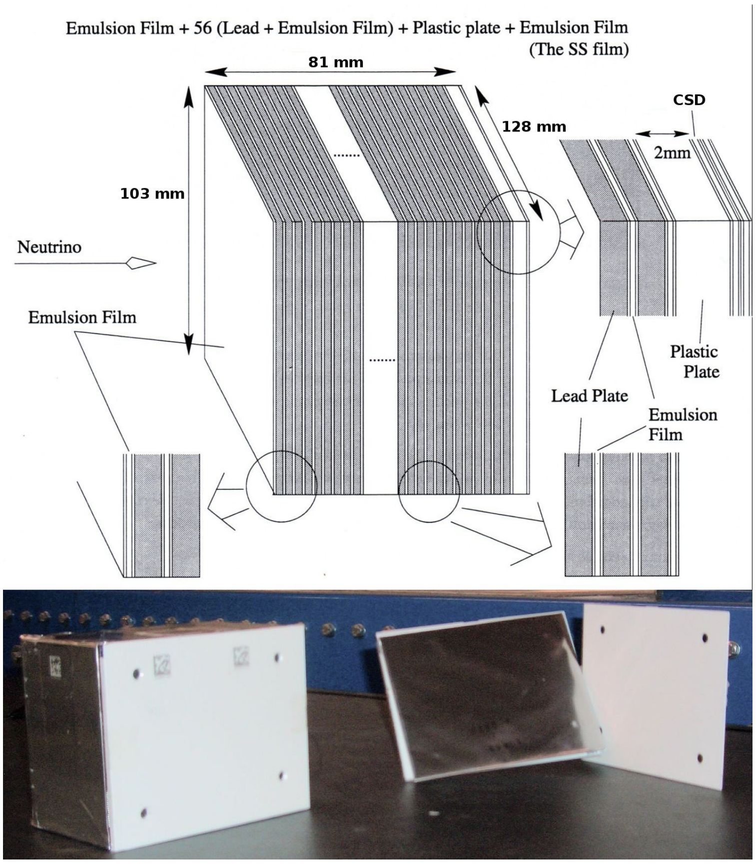

Figure 2.6: *ECC brick consisting of 57 emulsion films and 56 lead plates, plus two extra emulsion films forming the changeable sheet doublet. [45]*

The total emulsion target consists of 154750 bricks, which are assembled in 62 vertical walls, 31 per supermodule (see Fig.2.7). The walls are placed with a pitch of $124 mm$ along beam direction. The thickness of the wall structure is $85.6 mm$, so the distance between the walls is $38.4 mm$. This space then is filled with the electronic target tracker biplanes, each one coupled to an adjacent target wall[4]. The target walls are approximately square and each one contains 52 bricks horizontally and 64 bricks vertically. Though not all of the walls will be filled. The target filling strategy at the moment is to use 29 walls instead of 31 and fill only 51 rows instead of 64. Hence this amounts to a total of 2652 bricks and a total weight of about $23 ton$. The structure is made out of stainless steel to keep it light (about 0.4 the target) in order to limit as much as possible neutrino interactions in the target area outside the bricks themselves and to enable a small spatial separation between the bricks in all directions. The nominal size of the target area (inclusive clearances) is $6664.6 \times 6739.2 mm^2$. The bricks are positioned with the film plane perpendicular to the beam and with the long side of the film along the horizontal direction. The mechanical accuracy in brick positioning is of around $1mm$ [40, 45].

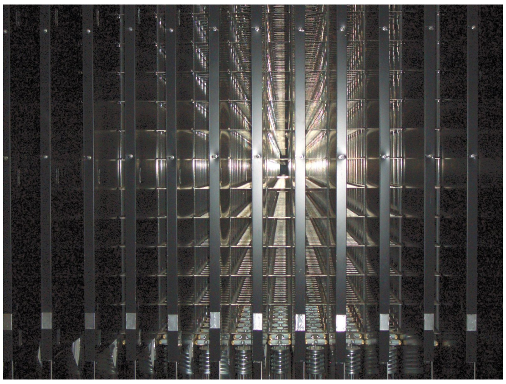

Figure 2.7: *Target brick wall with target tracker planes*

After a neutrino event takes place, electronic detectors show which brick holds the event. Then the selected brick gets extracted from the detector and will be exposed to cosmic rays for alignment reasons. The brick will be disassembled and the emulsion films developed and sent to the readout facilities. The event information gets extracted via scanning stations (automatic microscopes, see Fig.2.8).

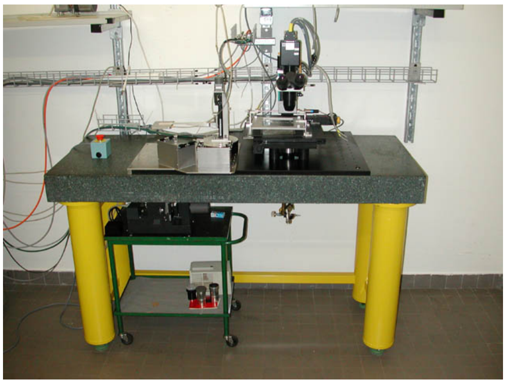

Figure 2.8: *Picture of one of the automatic microscopes needed to scan the events in the emulsion films.*

---

[4] see Chapter 2.3.2

2.3.2 The Target Tracker

The Target Tracker (TT) is placed between the target walls housing the bricks and covers a surface of about $3000m^2$. Its main role is to locate the brick in which a neutrino interaction occurred: A particle crossing a TT plane induces an electric signal. These signals are used to reconstruct the event (see Chapter 3.1). Knowing this we can locate the brick which holds the primary vertex of the neutrino interaction.

The brick finding efficiency is required to be high, therefore the TT's spatial resolution needs to be high as well. It is also needed that the TT shows long term stability and reliability, as it is extremely difficult to replace faulty elements and that in the case of problems the brick finding efficiency of not only the bricks in front but also on several walls upstream would be affected.

The TT is made up of plastic scintillator strips wich are $6.86m$ in length, $26.3mm$ in width, and $10.6mm$ thick. They are read using Wave Length Shifting (WLS) fibres and photodetectors (PMT), placed at both ends of the fibres. The detection principle for a crossing particle is shown in Fig.2.9. The track finding resolution is determined by the width of the scintillator strips and is therefore $26.3mm$. This detector is very reliable because the elements used are robust, and the more delicate elements, such as the electronics and the PMTs, are placed in accessible places.

A TT wall consists of two planes ($6.7 \times 6.7m^2$) with four modules each, one with vertical and one with horizontal strips, providing x-y information (see Fig.2.10a). A module has 64 strips which are read out by WLS fibres coupled to two 64-pixel photodetectors (see Fig.2.10b). The quantities for some TT detector components are given in Table 2.3.

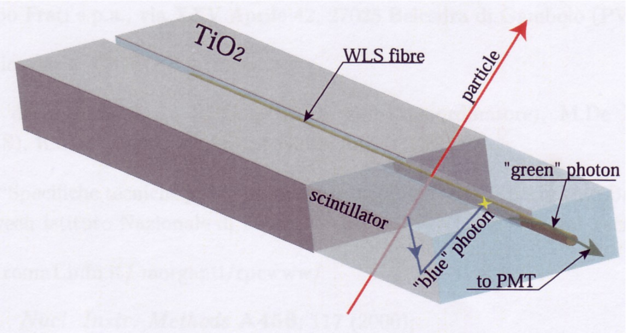

Figure 2.9: *Particle detection principle. The crossing particle produces a 'blue' photon which the WLS fibre changes to a 'green' one on its way to the PMT.*

Number of detector components	per plane	per wall	for the full detector
Scintillator modules	4	8	496
Scintillator planes	1	2	124
Scintillator strips	256	512	31744
PMTs	8	16	992

Table 2.3: *Summary of the main numbers for the TT.*

For several scintillator strip samples Fig.2.11 shows the number of photoelectrons (pe) versus the distance from the two PMTs. The worst case we get if the particle crosses the strip in the middle ($4.5m$ distance from both PMTs). Still the number of pe is well above 4 inducing a particle detection efficiency higher than 98% [40].

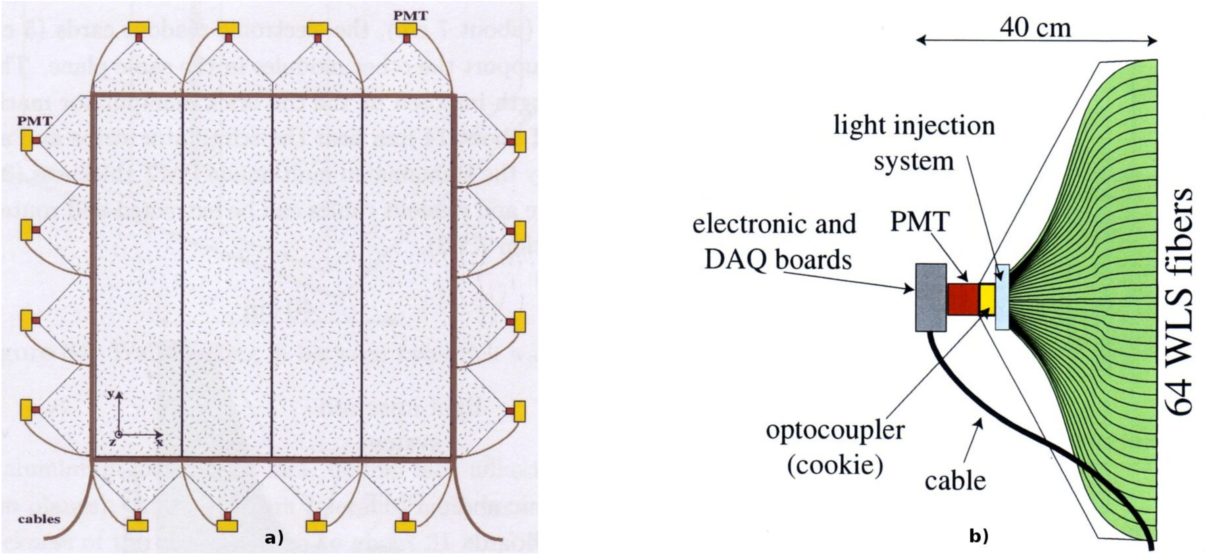

Figure 2.10: *a) TT wall consisting of two planes. Each plane is made up of four modules, one plane with vertical scintillator strips, the other one with horizontal strips, providing x-y-information. The signals are read out using Wave Length Shifting (WLS) fibres and photomultipliers (PMT). b) Schematic view of the WLS fibres and the PMT.*

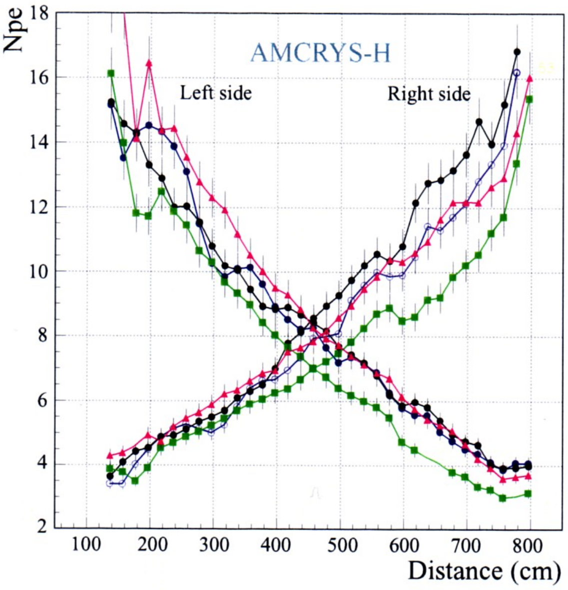

Figure 2.11: *Number of pe vs the distance from the PMTs for some scintillator strip samples.*

2.3.3 The muon spectrometers

Next to the ECC bricks and the TT, which build the target section, each supermodule includes a muon spectrometer. The spectrometers consist of a warm dipolar magnet and active detectors (RPC[5], XPC[6], and Drift Tubes). The magnet's shape is rectangular. It is made up of two vertical walls, each lining twelve iron layers of $5cm$ thickness, and of a top and bottom flux return path (see Fig.2.12). Between the iron layers are air gaps of $2cm$, allocated for RPCs. Each of these iron layers consists of seven slabs with dimension $50 \times 1250 \times 8200mm^3$. The overall weight of the magnet is $990ton$. The magnetisation of the dipole is done by two coils. Each coil is made up of 20 turns, where the ones in the upper return yoke are connected in series to the 20 turns in the bottom yoke. The nominal current flowing in these coils is $1600A$. This corresponds to an overall magnetomotive force of $6400A \times turns$. The average B field expected along the walls is $1.57\ T$. The uniformity along the height is better than 5%. Horizontally the uniformity strongly depends on the size of the air gaps as well as on the magnetic properties of the slab steel. The magnets are magnetically decoupled from the rest of the detector using stainless steel supports.

In measurements, the magnetic flux shows a systematic deficit smaller than 3%. This is due to the non-ideal mechanical contact and steel machining. Accounting for these corrections the average field is expected in the range $1.54 \div 1.57\ T$. However, during data taking the magnetic flux is measured in situ by the field monitoring system with a precision of a few per cent.

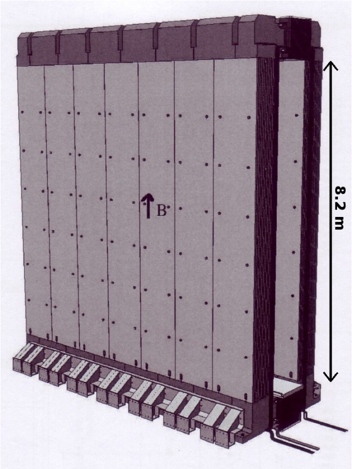

Figure 2.12: *One of the OPERA spectrometer magnets*

The Precision Tracker (PT) comprises the dipole magnets and the drift tubes. Its aim is not only to measure the muon momentum but as well to determine their sign. This is important in order to reject the background in the muonic tau decay channel. For this the efficiency should be 99% and the spatial resolution $300\mu m$. The detector has to cover the large area of $8 \times 8\ m^2$. To achieve this the detector wall was built out of thin walled aluminium tubes with an outer diameter of $38mm$ and a length of $7.9m$. Tube chambers with such long tubes have not been used so far which marked a challenge. The PT then was designed with special emphasis on

- mechanical robustness:
  for a reliable operation of the detector it was essential to have a high mechanical stability and a minimal number of parts.

---

[5] Resistive Plate Chamber

- chamber gas:
  to reduce possible sources of leakages one avoided to connect gas pipes to the individual tubes. Also the gas volume had to be free of glue in order to retain a high gas quality.
- wire positions:
  the wire positions have been made independent of the tube positions so as to avoid a pile up of inaccuracies. The tolerance on wire alignment should be less than $100\mu m$.
- signal quality:
  at the end of the tubes is a complete Faraday cage. All ground connections are qualified for high frequency.

The PT is composed of 9216 aluminium drift tubes, each with a central sense wire of $45\mu m$ diameter. The spectrometers are equipped with six fourfold layers of tubes each, grouped into 16 modules. Each module consists of 48 tubes with an outer diameter of $38mm$ and a wall thickness of $850\mu m$. The tubes are grouped in two by two rows, having an equal wire distance of $42mm$ in each row. In order to minimise the left/right ambiguities and to achieve an optimal geometrical acceptance, the layers are staggered. The tubes in a module are glued into nine aluminium sheets to obtain mechanical stability and exact positioning. A module is covered with plates at both ends which provide gas distribution and gas seal. These cover plates are also needed to position the wires with high precision.
The momentum resolution depends on the spatial resolution of the modules and on multiple scattering. The spatial resolution of one tube is $300\mu m$. A mean momentum of $6.482GeV$ entails a momentum resolution of $dp/p = 0.203$. The accuracy of the alignment over the whole module length is $100\mu m$.

The Inner Tracker is made up of Resistive Plate Chambers (RPC). The aim of the RPC system is to reconstruct tracks inside the magnet, identify penetrating muons, and measure their charge and momentum. All this independent of the PT. The high mass due to the iron of the magnet allows also beam monitoring. Ambiguities in the spatial track reconstruction are resolved by an RPC plane which completes each of the two drift tube planes of the PT upstream of the dipole magnet. These RPC planes are called XPCs and provide a precise timing signal to the PT as well.
Both the Inner Tracker and the XPCs are made of RPCs (see Fig.2.13). They have a high intrinsic and geometrical efficiency, are robust and flexible. The active area is filled with an argon-based gas mixture at atmospheric pressure. When a charged particle crosses the chamber, a spark is produced which induces signals on external pickup electrodes. Induced pulses are collected on two pickup strip planes. The strips of the Inner Trackers run in two orthogonal directions. Therefore they provide two-dimensional information. The vertical strips got a pitch of $26mm$ with $2mm$ separation, the horizontal ones a pitch of $35mm$ with a $2mm$ separation[6]. In the case of the XPCs, the strips are inclined of 43° with respect to the floor, the pitch is $26mm$, and the separation is $2mm$.
The induced charge is of the order of $100pC$. The pulse has a rise time of $2ns$ and a duration between $10ns$ and $20ns$ [7].
The active area of a dipole has the dimensions of $8m$ in height and $8.75m$ in width. We got two spectrometers with 22 gaps each. Therefore the total detector area is $3080m^2$. One gap is filled with seven RPCs in height and three RPCs in width. So in total there are 21 modules per gap (four different types, all of them have the dimensions $1.134m \times 2.91m$). Then the total number of RPC modules needed for both spectrometers is 924. As mentioned before there are two XPC planes

---

[6] Vertical and horizontal with respect to the floor where the detector is built.

[7] for a gas mixture composed of $Ar/C_2H_2F_4/i-C_4H_{10} = 48/48/4$ and for a voltage difference of $7.8kV$

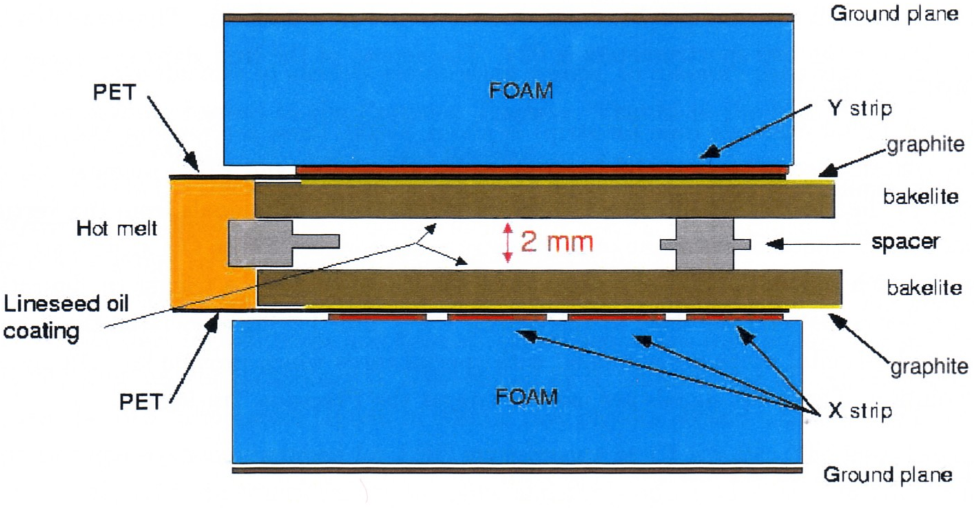

Figure 2.13: *Resistive Plate Chamber*

installed upstream of each dipole magnet. One directly attached on the magnet, the second one is placed with a distance of about $1m$ from the magnet. Each of the XPC walls needs 21 RPC modules (three different types, two with dimensions $1.134m \times 2.91m$, one with $1.134m \times 1.68$), hence the total number mounts up to 84.

There is one digital channel per strip, so the total amount is of about 25000 (see Table 2.4). The horizontal strips have 224 channels. The numbering is from bottom to top (channel number one is the lowest one). Vertically there are 336 channels, and the numbering is from right to left, seen in beam direction (see Fig.2.14) [40].

	Horizontal	Vertical
Number of strips (single plane)	224	336
Number of strips (sub-detector)	4928	7392
Total Number of strips	9856	14784

Table 2.4: *Muon spectrometer readout channels*

2.3.4 The veto system

CNGS neutrinos will not just interact with the detector but also with the rock and concrete surrounding the apparatus. Secondary particles produced in these interactions then will enter the detector and may induce signals which may lead to a large amount of erroneous brick extractions and needless scanning. To reduce these false signals, a VETO system has been installed in front of the detector. The VETO system consists of two walls of glass Resistive Plate Chambers (GRPC). A layer is composed of 8 horizontal rows, each one made of 4 chambers. Three of the chambers are $2.60m$ long and $1.14m$ wide, while the fourth is $2.20m \times 1.14m$. So the overall sensitive area from all 64 chambers is almost $200m^2$ - the VETO is the largest GRPC based detector. A picture is shown in Fig.2.15 [46, 47].

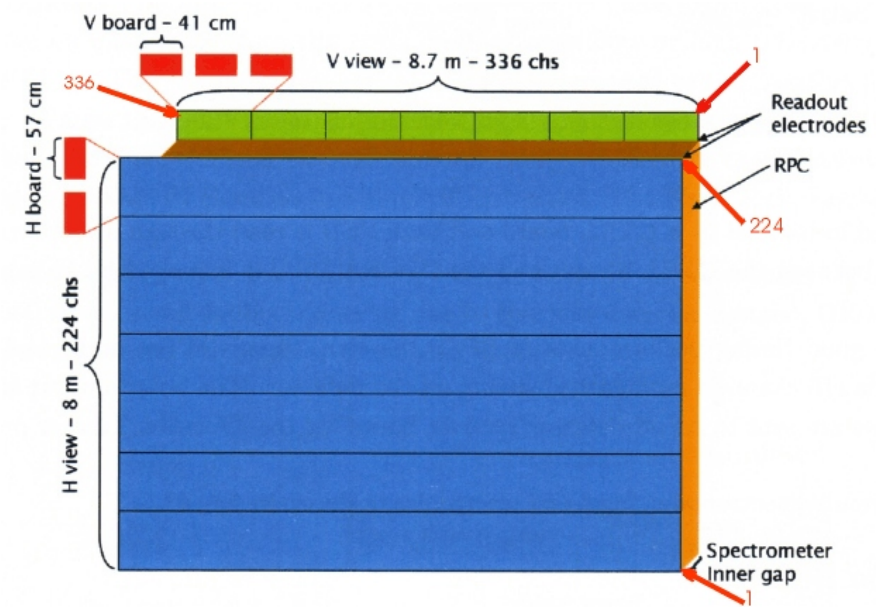

Figure 2.14: *Spectrometer RPC plane, seen in beam direction.*

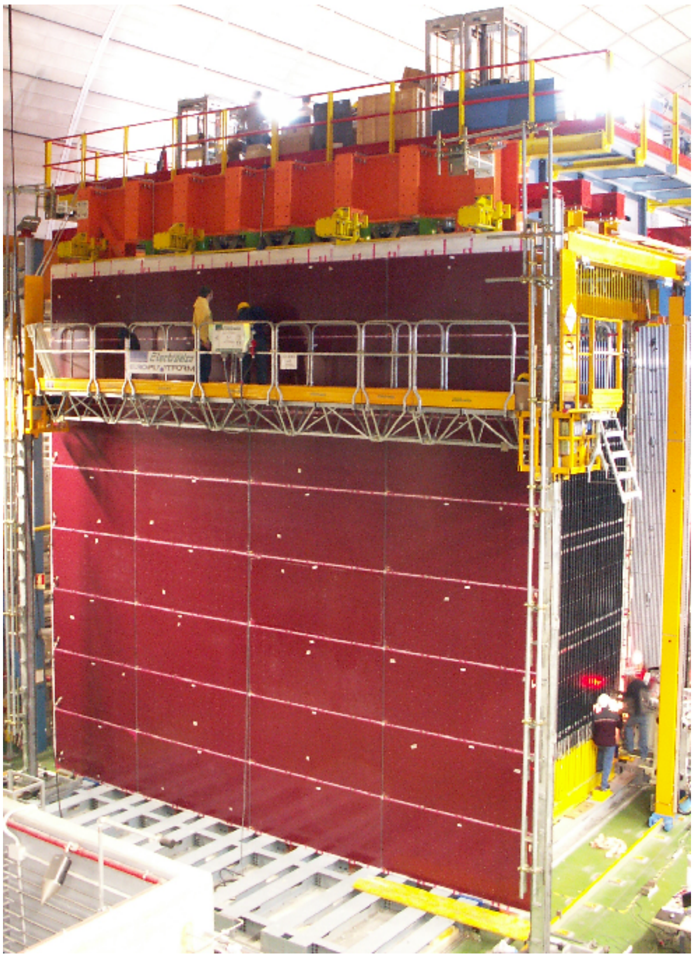

Figure 2.15: *VETO system in front of the detector made of GRPCs. [47]*

2.3.5 Data acquisition system (DAQ)

The data rate coming from neutrino interactions is low. Per day there are 46.45 ν_μ events in the whole detector, see Table 2.5. They are well localised in time correlated with the CNGS beam spill. The synchronisation with the CNGS beam is done offline by using the GPS. The detector even remains sensitive if there is no beam, though the DAQ system runs without a trigger. The events detected in a beamless time (mainly cosmic muons, background from radioactivity out of the proximity, dark counts) are used for monitoring of the detector.

Event type	number
NC	10.96
CC-DIS	31.42
CC-QE+RES	4.07
total	46.45

Table 2.5: *ν_μ events per day [48]*

The low data rate allows to sort the data through Ethernet at the earliest stage of each sub-detector. The global DAQ network (see Fig.2.16) is divided into two parts:

- The Ethernet network from the Event Building WorkStation (EBWS) to each Ethernet Controller (TT module, RPC plane, PT station). It is used for the detector configuration, monitoring and slow control[8], and data transfer.
- The clock distribution system from the Central Clock Unit synchronised on the GPS to each sensor.

In order to synchronise all the nodes of the distributed system a global clock is required. Bidirectionality is a characteristic feature of the system. It allows to control the reception of the signal and to measure the propagation time with an acknowledge signal. The clock distribution system starts with the GPS control unit. A $20MHz$ clock is synchronised using the GPS signal. The clock and encoded commands are sent via an optical fibre. Then the signal is converted into an electrical format and distributed to the Clock Master Cards. The Clock Master Cards deserialise the clock and the commands and distribute them to the clock unit of the controller boards.

Each time a particle produces a hit in one of the detectors, the time is automatically allocated to the hit in form of a timestamp. The timestamp is crucial to build an event. The event building sorts all in an acquisition cycle recorded hits in time and looks for time coincidence in a time window of typically $100ns$. An acquisition cycle is recorded in the form of a UTC (Universal Time Cycle) on the GPS control unit. The same procedure applies on the controller board, though a time delay appears. It depends on the actual position of the node in the detector and is due to the propagation delay from the control unit to the master card and from the master card to the node. A fast counter delays the cycle increment command according to the last measured value of time delay for the different nodes. So all the nodes begin their new acquisition cycle at the same absolute time with an accuracy of $10ns$. If a signal reaches the controller board, the value of the fast counter is put in a buffer, producing the timestamp. So all signals get their individual timestamp. Then the absolute time of an event is reconstructed by $T_{event} = T_{UTC} + T_{fastcounter}$.

All hits of an acquisition cycle now are time ordered for each node. To reconstruct an event, the lists of the recorded hits are gathered from all controller boards by the event building station and

---

[8] allows to view and change the status of the detector

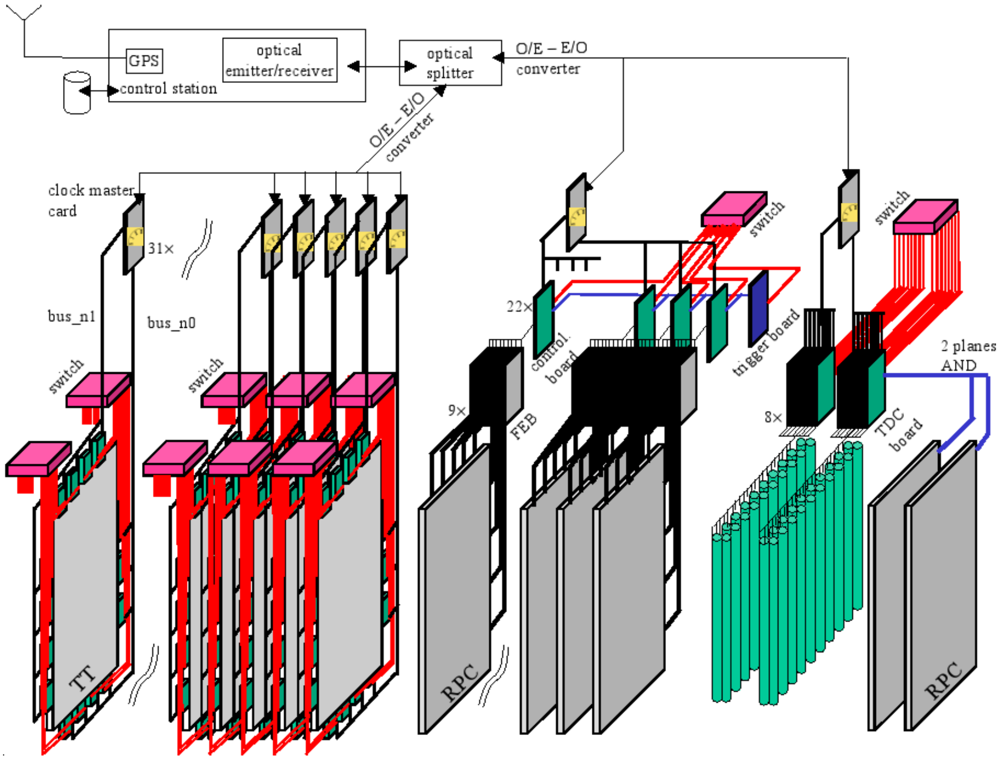

Figure 2.16: *Global DAQ scheme.*

sorted in time. In the next step the DAQ looks for time coincidences (time window around $100ns$) between the hits in a TT bi-plane and an RPC plane. For the TT it gets 62 hit lists and 44 for the spectrometer. All the remaining data are discarded. These hit lists then are searched for time coincidences between events in two different lists. All other sorts of cuts can be applied afterwards [40].

Chapter 3

Analysis methods

The sample of events we will use for our measurement are ν_μ CC interactions where a muon is produced plus other particles. First an event is just a package of hits which belong together. A hit is the electrical response of a particle crossing a detector. In order to give physical meaning to these hits, we pool them in tracks, each one coming from a single particle. The track finding problem is nicely solved by a Kalman Filter whose details will be described in the next paragraph. The fit evolving from this procedure is determined by five parameters: two spatial coordinates, two angles, and the ratio charge over momentum. The latter then leads to the energy of the muon.

Computer simulations of such events by means of Monte Carlo technique provide us with the information about the probability for a muon to have a certain energy given the energy of the interacting neutrino. Knowing this we can reverse it and so get the probability that a muon with a defined energy is found to be generated by a neutrino of a specific energy. This method is based on Bayes' Theorem that we will show in details in the next paragraphs. In the end we want to measure the neutrino flux that has generated the measured ν_μ CC events.

Our interest in measuring the neutrino flux is due to the fact that it is the main ingredient of any oscillation analysis. So the better we know the neutrino flux the better will be the estimate of the OPERA detector performance.

3.1 Kalman filtering

What we measure is the muon crossing the detector. The data which we are collecting is discrete. Now we want to estimate a fit of the muon track with its parameters. For this linear filtering problem for discrete data exists a recursive solution, the Kalman Filter. This is a set of mathematical equations which provides an efficient computational way to obtain the parameters of the fit of the muon track. The strength of this filter lies in the ability to support estimations of past, present, and future parameter states. This is even possible when the system, which is modelled, is not very well known.

In OPERA the tracking of muons takes place in heterogeneous structures (emulsions, RPCs, scintillators, drift tubes, ...). So the tracking method has to take into account the different types of detector measurements, moreover the local multiple scattering, energy losses, and magnetic field intensity. In the case of stopping muons one has to take care of the energy loss which strongly affects the kinetic energy and therefore the local curvature of the track (even more near the stopping point).

We got n measurements of the transverse spatial coordinates (x_i, y_i), $i = 1...n$, provided by some

detectors along the z-axis. Each measurement then is allocated a weight (w_{x_i}, w_{y_i}) which is the inverse of the spatial resolution squared. These points then can be either real or virtual measurement in case of simulated events. In a virtual measurement all the weights are set to 0. They are quite useful as being for example dummy steps which are needed to compute the energy loss and the local magnetic field intensity between two real measurements.
The fit of the muon track then is determined by 5 parameters:

$$x, \quad y, \quad a = \frac{p_x}{p_z}, \quad b = \frac{p_y}{p_z}, \quad d = \frac{q}{p} \tag{3.1}$$

where x and y are the coordinates, a and b are angles, $p_x,\ p_y,\ p_z$ are the components of the muon momentum $\overrightarrow{p}$, d is the curvature, and q is the charge. This set of parameters is referred to as **P**.
In order to compute these parameters we start at the end of the muon track. From this last point n we know all the parameters **P** from the initialisation, which we will show in details in a later paragraph. Knowing this, we start to estimate the parameters of the second last point and so on. So at the step i we take into account all information from the points from n to i into account to get the set of parameters for the next backward point $i-1$.
For this backward and progressive method we use all available information given by real measurements and by the knowledge of the characteristics of each of the different materials the muon crossed for data, and only the information given by the latter for simulations.

Matter effects such as energy loss and multiple scattering are decoupled from geometrical extrapolation. Multiple scattering is supposed to be an unbiased process, meaning that it does not affect the previous mean values $\mathbf{P}_i$. Energy loss on the other hand changes the parameter d_i into d_i^*

$$d_i^* = \frac{q_i}{\sqrt{E_i^*(E_i^* + 2m_\mu)}} \tag{3.2}$$

where $E_i^* = E_i + \triangle E_{i-1,i}(E_i^*)$ is the kinetic energy of the muon before passing through the material between z_i and z_{i-1}. $\triangle E_{i-1,i}(E_i^*)$ has to be computed iteratively because of its E_i^* dependency.
In practice GEANT[1] routines are used to compute energy losses. The convergence to get $\triangle E_{i-1,i}$ is reached with an accuracy of $10^{-4} GeV$ in 10 iterations for a sub-GeV muon crossing $1cm$ iron.

We now assume a homogeneous magnetic field. For the geometrical extrapolation of the coordinates we use Taylor expansions:

$$\begin{aligned} x_{i-1}^e &= x_i + a_i \triangle z_{i-1} + \frac{1}{2} A_i \triangle z_{i-1}^2 + ... \\ y_{i-1}^e &= y_i + b_i \triangle z_{i-1} + \frac{1}{2} B_i \triangle z_{i-1}^2 + ... \end{aligned} \tag{3.3}$$

and for the cosine directions

$$\begin{aligned} a_{i-1}^e &= a_i + A_i \triangle z_{i-1} + ... \\ b_{i-1}^e &= b_i + B_i \triangle z_{i-1} + ... \end{aligned} \tag{3.4}$$

---

[1] `http://geant4.web.cern.ch/geant4/`. GEANT is a tool which simulates the passage of particles through matter. It already includes a complete range of functionality such as tracking, geometry, physics models, and hits. The physics processes cover electromagnetic, hadronic, weak, and optical processes. It provides a lot of elements and materials for the particles to cross and interact within and covers a wide energy range from $250eV$ up to TeV. [50]

with $\triangle z_{i-1} = z_i - z_{i-1}$. A_i and B_i are calculated as follows:

$$\begin{aligned} A_i &= \frac{1}{cos\theta_i} d_i \left[b_i B_z + a_i b_i B_x - (1+a_i^2) B_y \right] \\ B_i &= \frac{1}{cos\theta_i} d_i \left[-a_i B_z - a_i b_i B_y + (1+b_i^2) B_x \right] \end{aligned} \tag{3.5}$$

where $cos\theta_i = (1 + a_i^2 + b_i^2)^{-1/2}$ and $\overrightarrow{B}$ is the magnetic field. The curvature is conserved.

$$d_{i-1}^e = d_i^* \tag{3.6}$$

The set of extrapolated parameters (Eq.(3.3), (3.4), (3.6)) can be written as

$$\mathbf{P}_{i-1}^e = F(\mathbf{P}_i) \tag{3.7}$$

The error matrix of $\mathbf{P}$ is $\mathbf{V} = \mathbf{W}^{-1}$. If there is no multiple scattering and no error on the energy loss determination, the weight matrix $\mathbf{W}_{i-1}^e$ can be computed via the error propagation theorem:

$$\mathbf{W}_{i-1}^e = \left(D_{i-1,i}^{-1} \right)^T \mathbf{W}_i D_{i-1,i}^{-1} \tag{3.8}$$

with

$$D_{i-1,i} \equiv \left(\frac{\partial \mathbf{P}_{i-1}^e}{\partial \mathbf{P}_i} \right)_{5\times 5} \tag{3.9}$$

If we take into account the multiple scattering and the energy loss fluctuations, $\mathbf{W}_i$ in Eq.(3.8) has to be changed into

$$\mathbf{W}_i \rightarrow \left[\mathbf{W}_i^{-1} + \mathbf{Q}_{i-1,i} \right]^{-1} \tag{3.10}$$

with

$$\mathbf{Q}_{i-1,i} = \begin{bmatrix} 0 & 0 & 0 & 0 & 0 \\ 0 & 0 & 0 & 0 & 0 \\ 0 & 0 & Q_{aa} & Q_{ab} & 0 \\ 0 & 0 & Q_{ab} & Q_{bb} & 0 \\ 0 & 0 & 0 & 0 & Q_{dd} \end{bmatrix} \tag{3.11}$$

The different factors stand for

$$\begin{aligned} Q_{aa} &= \delta\alpha_{MS}^2 (1 + a_i^2 + b_i^2)(1 + a_i^2) \\ Q_{bb} &= \delta\alpha_{MS}^2 (1 + a_i^2 + b_i^2)(1 + b_i^2) \\ Q_{ab} &= \delta\alpha_{MS}^2 (1 + a_i^2 + b_i^2) a_i b_i) \\ Q_{dd} &= \left(\frac{\partial d_i^*}{\partial E_i^*} \right)^2 \sigma^2(\triangle E_{i-1,i}) \end{aligned} \tag{3.12}$$

$\delta\alpha_{MS}^2$ is the variance of the scattering angles and can be taken directly from GEANT. The contribution of $\sigma^2(\triangle E_{i-1,i})$ to Q_{dd} is due to the variance of the path length and the variance of the dE/dx fluctuation. The latter usually dominates by a factor of around 10 and can be obtained using GEANT to simulate muons passing through different materials.

The above procedure iteratively yielded in the next point, $i - 1$. Now we only have to add it, performing the so called Kalman filtering method:

$$\begin{aligned} \mathbf{W}_{i-1}\mathbf{P}_{i-1} &= \mathbf{W}^e_{i-1}\mathbf{P}^e_{i-1} + w_{i-1}p_{i-1} \\ \mathbf{W}_{i-1} &= \mathbf{W}^e_{i-1} + w_{i-1} \end{aligned} \tag{3.13}$$

where $w_{i-1} = diag(w_{x_{i-1}}, w_{y_{i-1}}, 0, 0, 0)$ and $p_{i-1} = (x_{i-1}, y_{i-1}, 0, 0, 0)$.

Now we managed to integrate backwards different kinds of information along the muon track. What is still missing is the initialisation of this process, which is a delicate issue. The initialisation is different for stopping and outgoing muons. For outgoing muons we start the process at the end of the track. We use a minimal set of measurements to perform a geometrical fit. We assume that there is a constant magnetic field B_x in iron plates of width h_i. We alternately measure in X and Y scintillator bars of width h_s. In order to determine a straight line in the X-Z plane we need to measure two points. Three points are necessary for a parabola in the Y-Z plane. The mean magnetic field, $B_x \cdot \left(\frac{h_i}{h_i+h_s}\right)^2$, provides us the correspondence factor between the curvature and the parameter d. The sub-weight matrices are computed for both fits and the combination gives the weight matrix. So at the z position of the last measurement we now defined the parameters $\mathbf{P}_{ini}$ and the weight matrix $\mathbf{W}_{ini}$.

In the case of stopping muons we already benefit of having a point where the kinetic energy vanishes. We perform two straight line fits, one in the X-Z plane and one in the Y-Z plane. Out of these fits we get the first four parameters and their weight matrices. Using the different dE/dx estimations along the short track defined by the previous fit, we get a backward estimation for the kinetic energy. A rough global analysis of the track yields in the charge initialisation. In case of a constant magnetic field we use a straight line extrapolation from the beginning till the end of the track. For the initial value of the parameter d we get:

$$d_{ini} = \frac{q_{ini}}{\sqrt{E_{ini}(E_{ini} + 2m_\mu)}} \tag{3.14}$$

with the weight

$$W_{d_{ini}} = \left[\left(\frac{\partial d_{ini}}{\partial E_{ini}}\right)\sigma_{E_{ini}}\right]^2 \tag{3.15}$$

where $\sigma_{E_{ini}}$ comes from dE/dx fluctuation parametrisation [49].

3.2 Monte Carlo samples

In addition to the data events with their track information we need simulated events. The simulations are done using Monte Carlo methods. Here we used GEANT[2], a tool which simulates the passage of particles through matter.

For our purpose we need samples of neutrinos stopping in the magnet iron walls in the OPERA detector, in all the other iron, in the surrounding rock, in the shield made out of concrete, and in the various media of BOREXino[3] (water and pseudocumene).

We not only need samples of muon neutrino events in different materials but also of the various

---

[2] `http://geant4.web.cern.ch/geant4/`. See footnote 1 on page 40

[3] a solar neutrino detector in front of the OPERA detector

kinds of interactions (charged current, neutral current, quasi-elastic, and resonances). The naming convention of the MC files is:

$$numuXX\_YYYY\_NN\_reco.root$$

where *numu* stands for muon neutrinos, *reco* means that the events are reconstructed (the hits are sorted into events and tracks), and the replacement characters

- XX stand for the sort of interaction taking place,
- $YYYY$ stand for the material where the interaction takes place,
- NN stand for the number of simulated events.

See Table 3.1. The files are of the type *root*. ROOT[4] is an object-oriented data analysis framework provided by CERN.

XX	standing	$YYYY$	material	mass $[kton]$
cc	CC - DIS	BORD	BOREXino: pseudocumene	0.589704
qe	CC - QE	BORU	BOREXino: pseudocumene	0.589704
res	CC - RES	BOWD	BOREXino: water	1.6094
nc	NC	BOWU	BOREXino: water	0.84855
		CTFW	BOREXino: water	0.9408
		CTPC	BOREXino: pseudocumene	0.00367
		FOOT	rock	175.946633
		ROCK	rock	208.8959
		ROCS	rock	3128.7907
		WALL	rock	33.81568
		WALR	rock	33.819568
		BASL	rock	7.273024
		SHIELD	concrete	18.70966
		SLPL	magnet iron walls	1.355
		noSLPL	iron (but not in SLPL)	0.84

Table 3.1: *Meaning of the replacement characters XX and YYYY in the names of MC files. The sort of material is specified, together with the mass.*

These samples then have to be weighted according to the number of simulated and expected events and to the beam luminosity. We assume that all the materials are isoscalar ($Z = N$) except for iron. The cross-section for the CC deep inelastic scattering (DIS) is:

$$\sigma^{DIS}(E) = \sigma_0 \times E[GeV] = 0.677 \times 10^{-38} cm^2 \times E[GeV] \tag{3.16}$$

The total DIS cross-section then is the integral of the flux $\phi(E)$ times the cross-section over the integral of the flux:

$$\sigma_{tot}^{DIS} = \frac{\int \phi(E)\sigma^{DIS}(E)dE}{\int \phi(E)dE} = \frac{\int \phi(E)\sigma_0 E dE}{\int \phi(E)dE} = \sigma_0 \frac{\int \phi(E) E dE}{\int \phi(E)dE} = \sigma_0 \langle E \rangle \tag{3.17}$$

---

[4] `http://root.cern.ch/`

therefore σ_{tot}^{DIS} is

$$\sigma_{tot}^{DIS} = 0.677 \times 10^{-38} cm^2 \times \langle E[GeV] \rangle \tag{3.18}$$

For all the other interactions the cross-sections are considered to be constant for energies above $1GeV$. The quasi-elastic (QE) interaction $\nu_\mu + n \rightarrow \mu^- + p$ has the cross-section

$$\sigma^{QE} = 0.891 \times 10^{-38} cm^2 \tag{3.19}$$

For resonances (RES) we have three interactions with different cross-sections:

$$\nu_\mu + n \rightarrow \mu^- + p + \pi^0, \qquad \sigma_{n,\pi^0}^{RES} = 0.537 \times 10^{-38} cm^2 \tag{3.20}$$

$$\nu_\mu + n \rightarrow \mu^- + n + \pi^+, \qquad \sigma_{n,\pi^+}^{RES} = 0.276 \times 10^{-38} cm^2 \tag{3.21}$$

$$\nu_\mu + p \rightarrow \mu^- + p + \pi^+, \qquad \sigma_{p}^{RES} = 0.330 \times 10^{-38} cm^2 \tag{3.22}$$

The total cross-section for an isoscalar material is the sum of the cross-section σ_{tot}^{DIS}, which acts on both protons and neutrons, and of half of all the others as they act either on the proton or on the neutron:

$$\sigma_{iso}^{tot} = \sigma_{tot}^{DIS} + \frac{\sigma^{QE}}{2} + \frac{\sigma_n^{RES} + \sigma_p^{RES}}{2} \tag{3.23}$$

where $\sigma_n^{RES} = \sigma_{n,\pi^0}^{RES} + \sigma_{n,\pi^+}^{RES}$.

We now calculate the fraction for each process relative to σ_{iso}^{tot}.

$$f^{DIS} = \frac{\sigma_{tot}^{DIS}}{\sigma_{iso}^{tot}} \tag{3.24}$$

$$f^{QE} = \frac{\sigma^{QE}/2}{\sigma_{iso}^{tot}} \tag{3.25}$$

$$f^{RES} = \frac{(\sigma_n^{RES} + \sigma_p^{RES})/2}{\sigma_{iso}^{tot}} \tag{3.26}$$

$$f^{NC} = 0.3 \tag{3.27}$$

In the case of iron we have a non-isoscalar material. Therefore we need a correction for the cross-section and the fraction. Z is the proton number and N the neutron number. The atomic weight is about $A = Z + N$. The correction factors for QE and RES are the neutron or proton number over the number of nucleons, depending on whether the ν_μ interacts with a neutron or a proton.

$$\text{for neutrons: } \frac{N}{A} \quad ; \quad \text{for protons: } \frac{Z}{A} \tag{3.28}$$

For the DIS the correction factor is a bit more complex:

$$\frac{\sigma_n N + \sigma_p Z}{\sigma_{iso} A} \tag{3.29}$$

where σ_n is the cross-section of the ν_μ CC interaction on a neutron, σ_p on a proton, and σ_{iso} the cross-section on an isoscalar nucleus divided by the number of nucleons:

$$\sigma_{iso} = \frac{\sigma_n + \sigma_p}{2} \tag{3.30}$$

The ratio of the ν_μ cross-section on the neutron over the one on the proton is called R:

$$R = \frac{\sigma_n}{\sigma_p} \tag{3.31}$$

Therefore:

$$\frac{\left(\frac{\sigma_n}{\sigma_p}N+Z\right)\sigma_p}{\frac{\sigma_{iso}}{\sigma_p}\sigma_p A}=\frac{\frac{\sigma_n}{\sigma_p}N+Z}{\frac{1}{2}\left(\frac{\sigma_n}{\sigma_p}+1\right)A}=\frac{RN+Z}{0.5(R+1)A} \tag{3.32}$$

with $R = 2.04$, calculated by the NOMAD collaboration[5]. So the cross-sections for a non-isoscalar material look as follows:

$$\sigma^{DIS}_{noniso} = \sigma^{DIS}_{tot}\frac{RN+Z}{0.5(R+1)A} \tag{3.33}$$

$$\sigma^{QE}_{noniso} = \sigma^{QE}\frac{N}{A} \tag{3.34}$$

$$\sigma^{RES}_{noniso} = \sigma^{RES}_{n}\frac{N}{A}+\sigma^{RES}_{p}\frac{Z}{A} \tag{3.35}$$

The total cross-section for iron is the sum of the three single cross-sections:

$$\sigma^{tot}_{noniso} = \sigma^{DIS}_{noniso}+\sigma^{QE}_{noniso}+\sigma^{RES}_{noniso} \tag{3.36}$$

Again we calculate the fractions relative to the total cross-section σ^{tot}_{noniso}:

$$f^{DIS}_{noniso} = \frac{\sigma^{DIS}_{noniso}}{\sigma^{tot}_{noniso}} \tag{3.37}$$

$$f^{QE}_{noniso} = \frac{\sigma^{QE}_{noniso}}{\sigma^{tot}_{noniso}} \tag{3.38}$$

$$f^{RES}_{noniso} = \frac{\sigma^{RES}_{noniso}}{\sigma^{tot}_{noniso}} \tag{3.39}$$

We also need to take into account the various masses of the different volumes. They are listed in Table 3.1. The event rate is

$$rate = 604\ events/(kton \times 10^{19} pot) \tag{3.40}$$

Now we can calculate the number of expected events:

$$n^{\circ}\ of\ expected\ events = mass\ of\ material \times rate \times f \tag{3.41}$$

Together with the number of simulated events and the beam luminosity we get the weight for each file:

$$weight = n^{\circ}\ of\ expected\ events \times \frac{N_{pot}}{n^{\circ}\ of\ simulated\ events} \tag{3.42}$$

The numbers of simulated events are specified in Table 3.2. They total in 4103300 events. The beam luminosity, respectively the number of pot, for the run in autumn 2007 is

$$N_{pot} = 0.0824 \times 10^{19} pot \tag{3.43}$$

---

[5] Neutrino Oscillation MAgnetic Detector. Neutrino oscillation experiment at CERN from 1995-1998.

volume	cc	qe	res	nc
BORD	10k	10k	10k	
BORU	10k	10k	10k	
BOWD	50k	10k	10k	
BOWU	10k	10k	10k	
CTFW	1k	1k	1k	
CTPC	100	100	100	
FOOT	300k	100k	100k	
ROCK	300k	100k	100k	
ROCS	2M	100k	100k	
WALL	100k	50k	50k	
WALR	100k	50k	50k	
BASL	100k	10k	10k	
SHIELD	50k	25k	25k	25k
SLPL	15k	10k	10k	10k
noSLPL	20k	10k	10k	10k

Table 3.2: *Number of simulated events in diverse volumes for different interactions. Total number of simulated events: 4103300*

3.3 Producing histogramms

In order to analyse the data and MC event samples we extract all the information we are interested in and fill them in histogramms. For this we use the program MyAna, a software package of OPERA, based on ROOT[6]. MyAna allows us to read the data and MC files and to extract all the physical information about the 3-dimensional tracks. Within ROOT one can easily build histogramms.

We need to be careful with events holding more than one 3-dimensional track in order to avoid that these events produce more than one entry in the histogram. Therefore we only select the first and longest 3d track (*per definitionem* the muon track of the primary vertex). In the data files we also need to select the ontime events. Ontime means that the event happened during the time the CNGS beam was turned on and delivering neutrinos, therefore the event is not from a cosmic particle. This we know as every event got timestamped.

In the end we want to know the neutrino flux $\phi(E)$ whose derivative is connected to the interacting neutrinos via the cross-section:

$$\frac{dN}{dE} = \frac{d\phi}{dE}\sigma(E) \tag{3.44}$$

Thus the only physical variable we are interested in is the energy. So as to acquire the information about the energy we first extract the 3-dimensional tracks. As we are only interested in ν_μ CC events which produce a muon, we check each event if it holds a muon track. If so we read out the fifth parameter ($d = q/p$, see Chapter 3.1 about Kalman filtering). Then the energy of this muon is given by

$$E_\mu = \frac{1}{|d|} \tag{3.45}$$

---

[6] http://root .cern.ch/

The absolute value of d implies independence of the sign of the charge. The extraction of the muon energy is identical for data and the muons 'measured' in the MC. But the MC file not only provides us with the muon energy, it also holds the MC true information about the energy of the interacting neutrinos, E_ν.

Now we know the energy of the muons both for data and MC as well as the simulated neutrino energy. We arrange all this in three histogramms:

- the muon energy distribution from real neutrino events, $E_{\mu_{ontime}}$
- the energy distribution of the interacting neutrinos from the simulated events, E_ν
- a 2-dimensional histogram of the neutrino energy with respect to the muon energy from the simulated events, E_ν vs. E_μ

We used many MC files and therefore got just as many histogramms. What we need to do now is to merge the histogramms into a single one. In the previous section (Chapter 3.2) we showed how to calculate the weights for the different files. The average energy we get from the 2005 CNGS beam simulation[7]. Now we calculate the weights with $\langle E \rangle = 18.4 GeV$ and apply them on the histogramms. We add up the histogramms and get three single ones holding all the information needed for further studies.

3.4 Unfolding method based on Bayes' Theorem

Bayes' Theorem provides a way to get the best estimation of the real distribution by unfolding experimental distributions. As already mentioned in the introduction, this unfolding method allows us to get the information about the energies of the interacting neutrinos given the measured energy of the muons produced in neutrino interactions.

The only weak point of this method may be the fact that we need knowledge of the initial distribution. If necessary, this can be overcome by an iterative procedure. A strength of this method is that it does not use continuous variables but discrete cells in multi-dimensional histogramms, both of the true and measured quantities. The distributions of the true and measured observables are different due to physics and detector effects. So we need a good knowledge of the effect of all the distortions on the true physical quantity. The aim is to unfold the observed distribution from all the distortions in order to extract the true distribution.

The main advantages of this method compared to others are:

- it is theoretically sound
- it can be used to solve multidimensional problems
- it can take different sources of background into account (simply add it to the possible causes, see below)
- no matrix inversion, which is a problem present in unfolding procedures not based on Bayes' Theorem
- with a realistic guess of the distribution of the true values it yields best results, but even satisfactory results can be obtained starting from a uniform distribution

---

[7] available at http://www.mi.infn.it/∼psala/Icarus/cngs.html

- it provides the correlation matrix of the results

We now state Bayes' Theorem through several independent causes C_i, $i = 1...n_C$, which can produce one effect E. We further assume that we know the initial probability of the causes $P(C_i)$ as well as the conditional probability $P(E|C_i)$ that the i-th cause produces the effect. Then Bayes' formula looks like

$$P(C_i|E) = \frac{P(E|C_i)P(C_i)}{\sum_{l=1}^{n_C} P(E|C_l)P(C_l)} \tag{3.46}$$

In words: In the case that we observe the effect E, the probability that it happened due to the i-th cause is proportional to the probability of the cause itself times the probability of the cause to produce this effect.
The $P(C_i|E)$ depends on the initial probability of the causes. The Bayes formula has also the ability to increase the knowledge of $P(C_i)$ with the increasing number of observations. If we have no knowledge of $P(C_i)$ at all, the process can be started with a uniform distribution. $P(C_i|E)$ also depends on $P(E|C_i)$ which have to be calculated or estimated, respectively, by MC methods. Unlike the $P(C_i)$, these probabilities do not get updated by the observations.

We now observe $n(E)$ events with the effect E. $\hat{n}(C_i)$ is the expected number of events assigned to each cause.

$$\hat{n}(C_i) = n(E)P(C_i|E) \tag{3.47}$$

In a real measurement we usually have more than just one possible effect. For a given cause C_i we now have several possible effects E_j, $j = 1...n_E$, and for all of them Bayes' formula holds, and therefore we get

$$P(C_i|E_j) = \frac{P(E_j|C_i)P_0(C_i)}{\sum_{l=1}^{n_C} P(E_j|C_l)P_0(C_l)} \tag{3.48}$$

where $P_0(C_i)$ is the initial probability of the causes. These conditional probabilities $P(C_i|E_j)$ are referred to as smearing matrix $\mathbf{S}$. We remind of the following:

- $\sum_{i=1}^{n_C} P_0(C_i) = 1$
  This means, if the initial probability of a cause is 0 it cannot be changed, in other words, a cause who does not exist cannot be invented.
- $\sum_{i=1}^{n_C} P(C_i|E_j) = 1$
  This means that each effect has to come from one or more of the causes. So if there is a non-negligible amount of background contained in the observables, one has to include this in the causes.
- $0 \leq \epsilon_i \equiv \sum_{j=1}^{n_E} P(E_j|C_i) \leq 1$
  ϵ_i is the efficiency to detect the cause C_i in any of the possible effects. This means that there is no need for each cause to generate even one of the considered effects.

We take N_{obs} experimental observations and attain a distribution of frequencies

$$\mathbf{n}(E) \equiv \{n(E_1), n(E_2), ..., n(E_{n_E})\} \tag{3.49}$$

Applying Eq.(3.47) to each of the effects results in the expected number of events assigned to each of the causes due to observed events:

$$\hat{n}(C_i)|_{obs} = \sum_{j=1}^{n_E} n(E_j)P(C_i|E_j) \tag{3.50}$$

We take into account the inefficiency and get the best estimation of the true number of events.

$$\hat{n}(C_i) = \frac{1}{\epsilon_i} \sum_{j=1}^{n_E} n(E_j) P(C_i|E_j) \tag{3.51}$$

where $\epsilon_i \neq 0$. If $\epsilon_i = 0$, then we set $\hat{n}(C_i)$ to 0 because the experiment is not sensitive to the cause C_i. From these unfolded events we derive the true total number of events, the final probabilities of the causes and the overall efficiency:

$$\begin{aligned} \hat{N}_{true} &= \sum_{i=1}^{n_C} \hat{n}(C_i) \\ \hat{P}(C_i) \equiv P(C_i|\mathbf{n}(E)) &= \frac{\hat{n}(C_i)}{\hat{N}_{true}} \\ \hat{\epsilon} &= \frac{N_{obs}}{\hat{N}_{true}} \end{aligned} \tag{3.52}$$

$\hat{\epsilon}$ may be different from the efficiency ϵ_0 calculated from the reconstructed and generated MC events.

$$\epsilon_0 = \frac{N_{rec}}{\hat{N}_{gen}} = \frac{\sum_{i=1}^{n_C} \epsilon_i P_0(C_i)}{\sum_{i=1}^{n_C} P_0(C_i)} \tag{3.53}$$

Is the initial distribution $\mathbf{P}_0(C)$ not consistent with the data, then it will not agree with the final distribution $\hat{\mathbf{P}}(C)$. Therefore the closer the initial distribution is to the true one, the better is the agreement.
The distribution $\hat{\mathbf{P}}(C)$ is between $\mathbf{P}_0(C)$ and the true distribution. This implies to use an iterative procedure.

Once we obtained the unfolded distribution $\hat{\mathbf{n}}(C)$ and want to evaluate the uncertainties. To see all the sources of uncertainties we first rewrite Eq.(3.51) using Eq.(3.48) and the fact that $\epsilon_i = \sum_{j=1}^{n_E} P(E_j|C_i)$:

$$\hat{n}(C_i) = \sum_{j=1}^{n_E} M_{ij} n(E_j) \tag{3.54}$$

with

$$M_{ij} = \frac{P(C_i|E_j)}{\epsilon_i} = \frac{P(E_j|C_i)P_0(C_i)}{\left[\sum_{l=1}^{n_E} P(E_l|C_i)\right] \cdot \left[\sum_{l=1}^{n_C} P(E_j|C_l)P_0(C_l)\right]} \tag{3.55}$$

M_{ij} is the unfolding matrix $\mathbf{M}$. The covariance matrix $\mathbf{V}$ of the unfolded numbers $\hat{n}(C_i)$ is the sum of various contributions:

- $P_0(C_i)$
  The initial probabilities are assumed to be without statistical errors because they solely influence the results systematically.

- $n(E_j)$
  The true number of events is estimated by $\hat{N}_{true}$. The data sample is distributed multinomially with the parameter n which is defined by the true number of events. The $\mathbf{n}(E)$ contribution to $\mathbf{V}$ is

$$V_{kl}(\mathbf{n}(E)) = \sum_{j=1}^{n_E} M_{kj} M_{lj} n(E_j) \left(1 - \frac{n(E_j)}{\hat{N}_{true}}\right) - \sum_{\substack{i,j=1 \\ i \neq j}}^{n_E} M_{ki} M_{lj} \frac{n(E_i) n(E_j)}{\hat{N}_{true}} \tag{3.56}$$

- $P(E_j|C_i)$
  These probabilities are estimated via Monte Carlo and show statistical and systematical errors. The systematic errors are due to assumptions made in the simulation. The statistical errors come from the limited number of simulated events and induce correlations between the results. If a cause C_i is observed only in a few effect-cells E_j and the number of generated events is not very large, we cannot neglect the covariance between $P(E_{j_1}|C_i)$ and $P(E_{j_2}|C_i)$. However, we can neglect it between terms with different causes. Then the contribution to $\mathbf{V}$ is

$$V_{kl}(M) = \sum_{i,j=1}^{n_E} n(E_i)n(E_j)Cov(M_{ki}, M_{lj}) \tag{3.57}$$

  where

$$Cov(M_{ki}, M_{lj}) = \sum_{\{ru\},\{su\}} \frac{\partial M_{ki}}{\partial P(E_r|C_u)} \cdot \frac{\partial M_{ij}}{\partial P(E_s|C_u)} \cdot Cov\left[P(E_r|C_u), P(E_s|C_u)\right] \tag{3.58}$$

  and

$$\begin{aligned} \frac{\partial M_{ki}}{\partial P(E_r|C_u)} &= M_{ki}\left[\frac{\delta_{ku}\delta_{ri}}{P(E_r|C_u)} - \frac{\delta_{ku}}{\epsilon_u} - \frac{\delta_{ri}M_{ui}\epsilon_u}{P(E_i|C_u)}\right] && (3.59) \\ Cov\left[P(E_r|C_u), P(E_s|C_u)\right] &= \begin{cases} \frac{1}{n_u}P(E_r|C_u)\cdot\left[1 - P(E_r|C_u)\right] & (r = s) \\ -\frac{1}{n_u}P(E_r|C_u)P(E_s|C_u) & (r \neq s) \end{cases} && (3.60) \end{aligned}$$

  n_u is the number of events generated in the cell C_u.

The covariance matrix of the unfolded numbers is the sum of the two contributions due to $n(E_j)$ and $P(E_j|C_i)$:

$$V_{kl} = V_{kl}(\mathbf{n}(E)) + V_{kl}(\mathbf{M}) \tag{3.61}$$

The use of Bayes' Theorem in a recursive way is a promising method which is able to unfold multidimensional distributions. It also provides the covariance matrix of the result. A Monte Carlo study has shown that this method does not bias the results [51].

Chapter 4

Physical results

The aim of this procedure is to unfold the CNGS neutrino flux ϕ. According to Eq.(3.44) we divide the flux of the interacting neutrinos $\frac{dN}{dE}$ by the cross-section $\sigma(E)$. The flux of the interacting neutrinos we get using the unfolding method described in Chapter 3.4. The expected number of events assigned to each cause is given by Eq.(3.54) with C standing for the neutrino energy E_ν and E for the muon energy E_μ:

$$\hat{n}(E_{\nu_i}) = \sum_{j=1}^{n_{E_\mu}} M_{ij} n(E_{\mu_j}) \tag{4.1}$$

where $\mathbf{M}$ is the unfolding matrix and n is the number of events. Now we first produce the three histogramms mentioned before:

- *HEmuot* is the muon energy distribution from real neutrino events
- *HEnu* is the energy distribution of the interacting neutrinos from the simulated events
- *HEmuEnu* is the 2-dimensional histogram of the neutrino energy with respect to the muon energy from the simulated events

See Fig.4.1. They all need to have the same normalisation. We chose 60 bins and an energy range from 0 to 180 GeV. This results in 3 GeV per bin.

In Eq.(4.1), $n(E_\mu)$ is the number of events in the real data. So this information is stored in the histogram *HEmuot*: $n(E_{\mu_j})$ is the number of entries in the j-th bin.

The unfolding matrix element M_{ij} is the probability that the measured muon j of energy E_{μ_j} was generated by the neutrino E_{ν_i} divided by the efficiency:

$$M_{ij} = \frac{P(E_{\nu_i}|E_{\mu_j})}{\epsilon_i} \tag{4.2}$$

The numerator is given by Eq.(3.48):

$$P(E_{\nu_i}|E_{\mu_j}) = \frac{P(E_{\mu_j}|E_{\nu_i})P_0(E_{\nu_i})}{\sum_{l=1}^{n_{E_\nu}} P(E_{\mu_j}|E_{\nu_l})P_0(E_{\nu_l})} \tag{4.3}$$

We get the initial probability $P_0(E_{\nu_i})$ from the histogram *HEnu*:

$$P_0(E_{\nu_i}) = \frac{n^\circ\ of\ entries\ in\ bin\ i}{total\ n^\circ\ of\ entries} \tag{4.4}$$

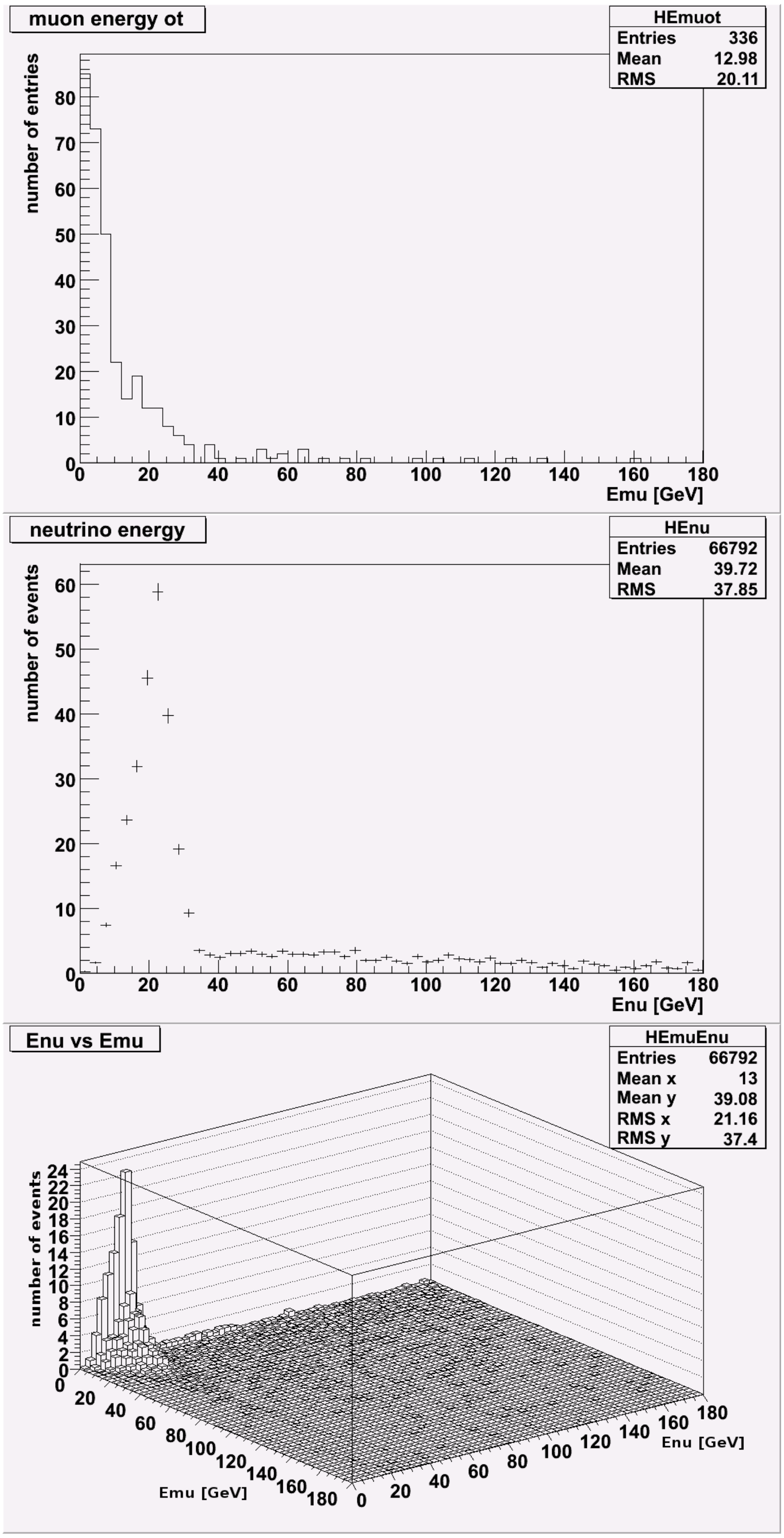

Figure 4.1: *top: muon energy distribution from CNGS neutrino events; middle: energy distribution of the interacting neutrinos from the simulated MC events; bottom: neutrino energy distribution (Enu) with respect to the muon energy distribution (Emu) from the simulated MC events*

The probability that a muon j has a certain energy given the energy of the interacting neutrino i, $P(E_{\mu_j}|E_{\nu_i})$, is the fraction of the probability of the intersection of E_{μ_j} and E_{ν_i} divided by the probability that the neutrino has the energy E_{ν_i}.

$$P(E_{\mu_j}|E_{\nu_i}) = \frac{P(E_{\mu_j} \cap E_{\nu_i})}{P_0(E_{\nu_i})} \tag{4.5}$$

$P(E_{\mu_j} \cap E_{\nu_i})$ we get from the histogram $HEmuEnu$.
The efficiency in Eq.(4.2) is

$$\epsilon_i = \sum_{j=1}^{n_{E_\mu}} P(E_{\mu_j}|E_{\nu_i}) \tag{4.6}$$

Now we have everything we need in order to calculate the flux of the interacting neutrinos. We fill the histogram $unfolded0$, see Fig.4.2.

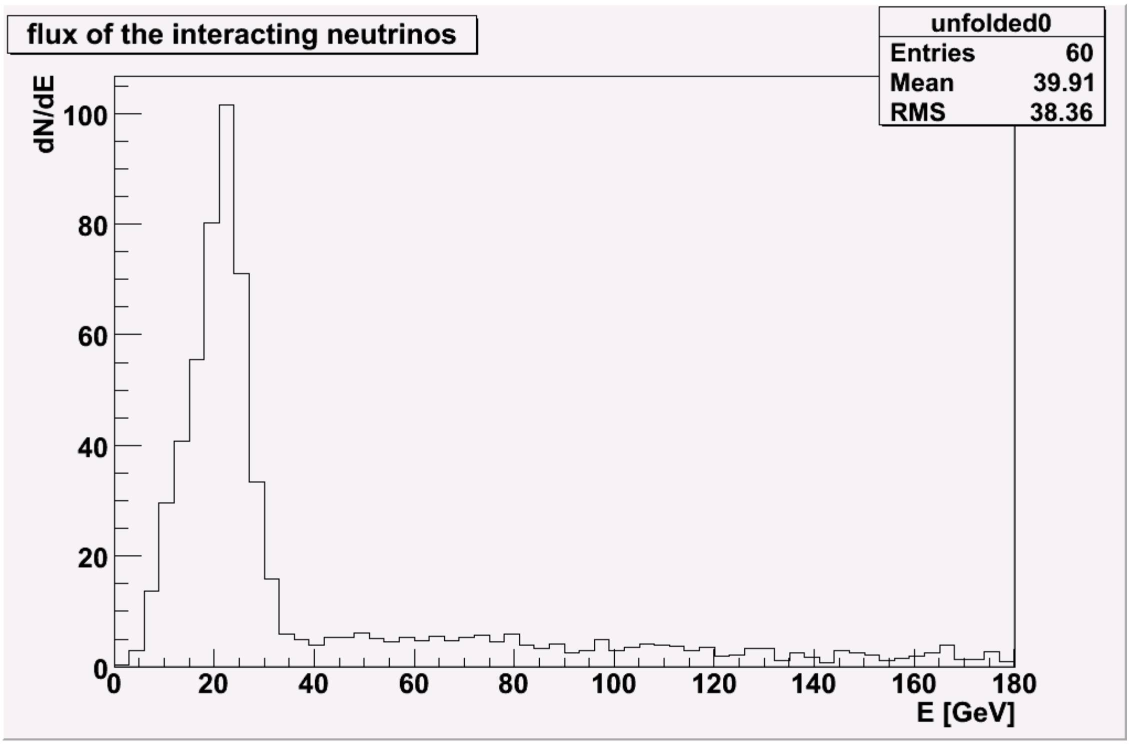

Figure 4.2: *Unfolded flux of the interacting neutrinos,* $\frac{dN}{dE}$

According to Eq.(3.44) the flux of interacting neutrinos, $\frac{dN}{dE}$, needs to be divided by the cross-section $\sigma(E)$ in order to get the neutrino flux $\frac{d\phi}{dE}$. The cross-section depends on the energy and is calculated the same way as in Eq.(3.23). For $E[GeV]$ we put the average energy of each bin.

$$\sigma(E) = 0.677 \times 10^{-38} cm^2 \times E[GeV] + 1.017 \times 10^{-38} cm^2 \tag{4.7}$$

So we divide the histogram $unfolded0$ bin-by-bin by the corresponding $\sigma(E)$. We store the unfolded neutrino flux in the histogram $unfoldedw$. See the red curve in Fig.4.3.

In OPERA the sensitivity is optimised to the atmospheric neutrino oscillation signal measured by Super-Kamiokande. This means we use $\triangle m^2_{23} = 2.4 \times 10^{-3}\ eV^2$ at full mixing in $\nu_\mu \leftrightarrow \nu_\tau$ oscillations

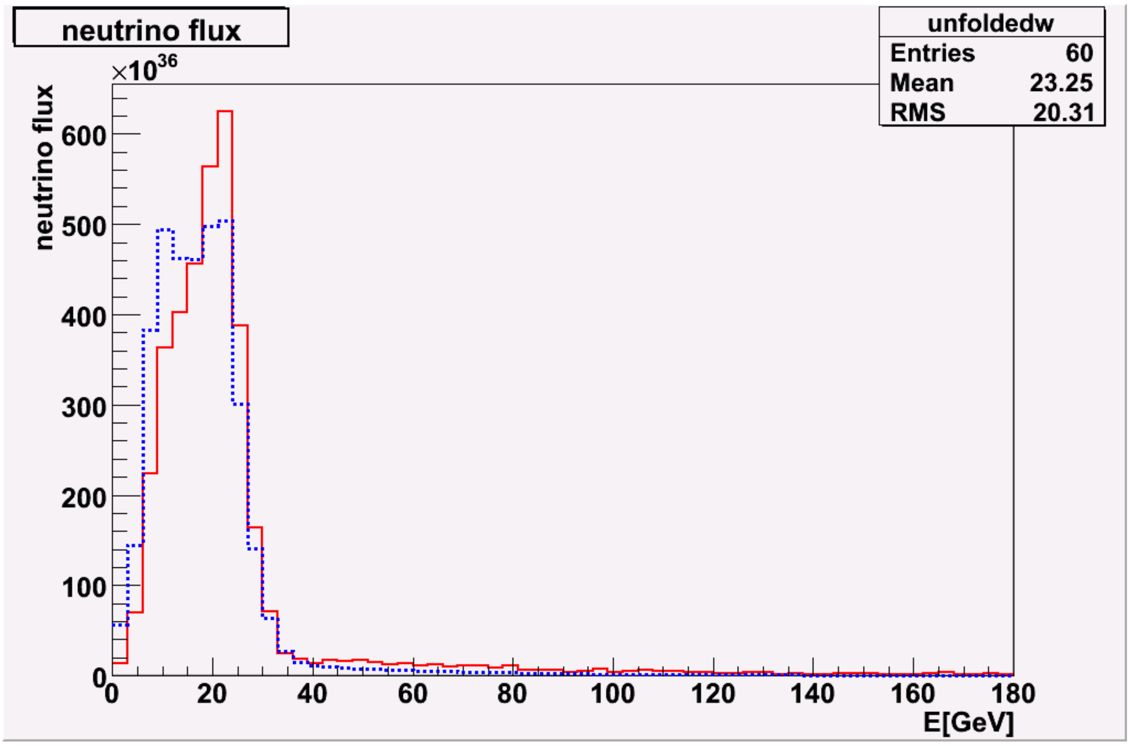

Figure 4.3: *Comparison of the unfolded CNGS neutrino flux (red, average energy 23.25 GeV) with the CNGS neutrino flux simulation of the year 2005 (blue, average energy 18.4 GeV).*

($sin^2 2\theta_{23} = 1.0$) [35]. We calculate the oscillation probability according to Eq.(1.34):

$$P(\nu_\mu \to \nu_\tau) = sin^2 2\theta_{23} sin^2 \left(1.27 \triangle m^2_{23} \left[eV^2\right] \frac{L\,[km]}{E\,[GeV]}\right) \tag{4.8}$$

The distance is $L = 732km$. The average energy of the unfolded neutrino flux distribution is $23.25\ GeV$. For this energy we get

$$P(\nu_\mu \to \nu_\tau) = 0.0092 \approx 1\% \tag{4.9}$$

In our distribution we did not include the oscillation probability as it has a negligibly small influence on the outcome.

Now we want to compare our unfolded neutrino flux with the neutrino beam simulation from the year 2005[1]. We normalise it according to the histogram $unfoldedw$. For this we multiply the content of the bin by the total number of entries of the histogram showing the unfolded neutrino flux, $unfoldedw$, and divide it by the total number of entries of the histogram with the simulated neutrino flux. We compare the histogram showing the simulated neutrino flux with the one showing the unfolded neutrino flux, see Fig.4.3.

This is the first attempt to measure the CNGS neutrino flux. From the measured muon momentum we obtain the neutrino energy distribution by using the unfolding method based on Bayes' Theorem. The unfolded distribution has its peak in the same bin as expected from the beam simulation. We

---

[1] available at http://www.mi.infn.it/~psala/Icarus/cngs.html

are quite satisfied of this result even if there is a clear disagreement in the shape.

We make a χ^2-test in order to estimate our fit. We calculate it as follows:

$$\chi^2 = \sum_{i=1}^{N_{sim}} \frac{(n_{unf_i} - n_{sim_i})^2}{n_{unf_i} + n_{sim_i}} \tag{4.10}$$

where n_{unf_i} is the content of the i-th bin of $unfoldedw$ and n_{sim_i} is the content of the i-th bin of the simulated neutrino flux. We obtain a value of 225 and the degree of freedom is $n = 60$. With such a high degree of freedom the distribution becomes a Gaussian. Then the mean value is n and the variance is $\sigma^2 = 2n$. Therefore the standard deviation is $\sigma = \sqrt{2n} = 10.95$. Our χ^2 is the mean value plus 15σ. This large χ^2 indicates that the disagreement is not just from statistical fluctuations but actually is evidence for a different shape.

For this disagreement, there are several possible explanations which stand to reason:

- Though the efficiency of the detector is included in the correlation matrix, the simulation of the detector may not be perfect, as low energetic muons are not efficiently reconstructed.
- Sine we are merging various samples of simulated neutrino interaction events in different materials for our statistics, some of these may be simulated wrongly. Hence MC simulations need to be further investigated.
- Even worse than the last point would be files missing completely. This would badly affect the statistics.
- Assuming the MC event samples to be correct and complete, there would still be the risk to weigh them in a non-optimal way while merging. Though a material specific cross-section was used for the production of the samples, for the merging we calculated the weights by using just one cross-section for all the different materials.
- Another contribution to this disagreement might come frome the not perfect simulation of the beam. It suggests itself that the beam simulation needs further investigation.

Conclusion

The OPERA detector is especially designed to search for the appearance of ν_τ within an almost pure ν_μ beam of the CERN to Gran Sasso facility (CNGS). This would be the first detection of the direct appearance of a ν_τ coming from ν_μ oscillation and thus the final confirmation that neutrinos oscillate and that they are therefore massive particles. The performance of the experiment strongly depends on the neutrino flux and on its knowledge. In this study, a neutrino flux determination of the CNGS was undertaken by exploiting a first set of data collected in the OPERA run of 2007. This is the first attempt to measure the CNGS neutrino flux. For this purpose we measure the momentum of muons produced in ν_μ charged current interactions. From the measured muon momentum we obtain the initial neutrino energy distribution by using an unfolding method based on Bayes' Theorem.

All the analysis done here relies on the comparison between data and simulated Monte Carlo (MC) events. As already mentioned, we only selected events coming from ν_μ charged current interactions which produce a muon. What we measure are the induced hits of the muon crossing the electronic detectors of the experimet. In order to give physical meaning to this set of hits, we pool them in tracks, each one coming from a single particle. This we do by means of a Kalman Filter algorithm. The Kalman Filter is a recursive solution to a linear filtering problem for discrete data providing an efficient computational way to obtain the parameters of the fit of the muon track which is determined by five parameters: two spatial coordinates, two angles, and the ratio charge over momentum. The latter then leads to the energy of the muon. Then we extract the muon energy for all the events, data and simulated ones. The MC simulations not only provide us the muon energy, they also hold the MC true information about the energy of the interacting neutrinos. The energy distributions of the muons from real events and of the interacting neutrinos from simulated events, and the correlation of the neutrino energy and muon energy of the simulated events, provide histogramms needed in order to unfold the neutrino flux by means of the unfolding method based on Bayes' Theorem.

Bayes' Theorem provides a way to obtain the best estimation of the real distribution by unfolding experimental distributions. This unfolding method allows us to get the information about the energies of the interacting neutrinos given the measured energy of the muons produced in neutrino interactions. The two-dimensional histogram of the neutrino energy with respect to the muon energy (from the simulated events) together with the energy distribution of the interacting neutrinos provide us the probability that a muon has a certain energy given the energy of the interacting neutrino, $P(E_\mu|E_\nu)$. This probability and the knowledge of the initial probability of the energy of the neutrinos gives the knowledge of the probability that a muon with a defined energy is found to be generated by a neutrino of a specific energy, $P(E_\nu|E_\mu)$. With this knowledge we can unfold the flux of the interacting neutrinos, that, divided by the cross-section, yields the actual neutrino flux.

The present Diploma Thesis is organised in four chapters:

- The first chapter gives general information on particle physics and of neutrino physics, with emphasis on the physics of oscillating neutrinos.
- A detailed description of the OPERA experiment can be found in the second chapter. Electronic detectors, which were important for this work, are described in detail as well as the CNGS neutrino beam.
- In the third chapter we describe methods used for the analysis such us Kalman Filtering and the unfolding method based on Bayes' Theorem. There are also details listed about the MC event samples.
- In the final chapter the performed analysis is shown and the results presented.

The unfolded neutrino flux spectrum shows the behaviour expected from the simulations. The agreement is satisfactory in particular as far as the peak neutrino energy is concerned. This first attempt will open the way to more detailed studies that will be performed when a higher statistics will be available from the experiment data taking.

Appendix A

Two flavour neutrino oscillation in vacuum

Eq.(A.1) is the probability of a neutrino of flavour α to change into a neutrino of flavour β ($\beta \neq \alpha$) after propagating over the length L.

$$\begin{align*}
P(\nu_\alpha \rightarrow \nu_\beta) &= |\langle \nu_\beta(0)|\nu_\alpha(L)\rangle|^2 \tag{A.1}\\
&= \left|\sum_i U^\dagger_{\alpha i} e^{-i\frac{m_i^2}{2}\frac{L}{E}} \langle \nu_\beta(0)|\nu_i(0)\rangle \right|^2\\
&= \left|\sum_{i,j} U^\dagger_{\alpha i} U_{j\beta} e^{-i\frac{m_i^2}{2}\frac{L}{E}} \langle \nu_j(0)|\nu_i(0)\rangle \right|^2\\
&= \left|\sum_i U^\dagger_{\alpha i} U_{i\beta} e^{-i\frac{m_i^2}{2}\frac{L}{E}} \right|^2\\
&= \left|\sum_i U^\dagger_{\alpha i} U^\dagger_{\beta i} e^{-i\frac{m_i^2}{2}\frac{L}{E}} \right|^2\\
&= \left| cos\theta sin\theta \left(e^{-i\frac{m_i^2}{2}\frac{L}{E}} - e^{-i\frac{m_j^2}{2}\frac{L}{E}} \right) \right|^2\\
&= cos^2\theta sin^2\theta \left(e^{-i\frac{m_i^2}{2}\frac{L}{E}} - e^{-i\frac{m_j^2}{2}\frac{L}{E}} \right) \left(e^{i\frac{m_i^2}{2}\frac{L}{E}} - e^{i\frac{m_j^2}{2}\frac{L}{E}} \right)\\
&= cos^2\theta sin^2\theta \left(2 - e^{-i\frac{\triangle m_{ij}^2}{2}\frac{L}{E}} - e^{i\frac{\triangle m_{ij}^2}{2}\frac{L}{E}} \right) \tag{A.2}\\
&= cos^2\theta sin^2\theta \left[2 - 2cos\left(\frac{\triangle m_{ij}^2}{2}\frac{L}{E} \right) \right] \tag{A.3}\\
&= \frac{1}{4} sin^2 2\theta \left[2 - 2cos\left(\frac{\triangle m_{ij}^2}{2}\frac{L}{E} \right) \right] \tag{A.4}\\
&= sin^2 2\theta \left[\frac{1 - cos\left(\frac{\triangle m_{ij}^2}{2}\frac{L}{E} \right)}{2} \right] \tag{A.5}\\
&= sin^2 2\theta sin^2 \left(\frac{\triangle m_{ij}^2}{4}\frac{L}{E} \right) \tag{A.6}
\end{align*}$$

We define $\triangle m_{ij}^2 \equiv m_i^2 - m_j^2$ and apply $\frac{1}{2}\left(e^{-ix} + e^{+ix}\right) = cos(x)$ on Eq.(A.2) in order to get Eq.(A.3). On the latter equation we use $4sin^2(\alpha) \cdot cos^2(\alpha) = sin^2(2\alpha)$.
So as to get to Eq.(A.5) from Eq.(A.6), we need to apply $\frac{1-cos(\alpha)}{2} = sin^2\frac{\alpha}{2}$.
To get a more convenient formula, one uses natural units:

$$c = \hbar = \epsilon_0 = 1 \tag{A.7}$$

This entails

$$\hbar c = 197.3MeV \cdot fm \hat{=} 1 \tag{A.8}$$
$$1m = 10^{15}\frac{1}{197.3}MeV^{-1} = 5.068 \cdot 10^{15}GeV^{-1} \tag{A.9}$$

For the mass we use the unit eV:

$$E = mc^2 \tag{A.10}$$
$$[m] = eV \tag{A.11}$$

So we use these units for the variables in Eq.(A.6)

$$\left[\triangle m_{ij}^2\right] = eV^2 \tag{A.12}$$
$$[L] = km \tag{A.13}$$
$$[E] = GeV \tag{A.14}$$

and get

$$\left[\frac{\triangle m_{ij}^2\left[eV^2\right]}{4}\frac{L\,[km]}{E\,[GeV]}\right] = \frac{eV^2}{4}\frac{5.068 \cdot 10^{18}GeV^{-1}}{GeV} \approx 1.27 \tag{A.15}$$

Then Eq.(A.6) becomes

$$P(\nu_\alpha \to \nu_\beta) = sin^2 2\theta sin^2\left(1.27\triangle m_{ij}^2\left[eV^2\right]\frac{L\,[km]}{E\,[GeV]}\right) \tag{A.16}$$

Notice the proportionality to $\frac{L}{E}$ [30].

The oscillation length L_{osc} is the length a neutrino of flavour α has to traverse in order to be in the same state as in the beginning (α). In vacuum we get it while setting the second part of Eq.(A.16) to zero:

$$sin^2\left(1.27\triangle m_{ij}^2\left[eV^2\right]\frac{L_{osc}\,[km]}{E\,[GeV]}\right) = 0 \tag{A.17}$$

and therefor

$$1.27\triangle m_{ij}^2\left[eV^2\right]\frac{L_{osc}\,[km]}{E\,[GeV]} = \pi \tag{A.18}$$

which results in [36]:

$$L_{osc}\,[km] = 2.48\frac{E\,[GeV]}{\triangle m_{ij}^2\left[eV^2\right]} \tag{A.19}$$

Acknowledgement

Thanks to...

... Prof. Antonio Ereditato and Prof. Urs Moser.

... Dr. Stefano Dusini from the University of Padova for his great support, all the discussions and help.

... Dr. Marcello Messina for expert advice and mentoring.

... Dr. Igor Kreslo, Dr. Ciro Pistillo, Dr. Sigve Haug, and Dr. Borge Gjelsten for the discussions on physics and support in computing.

... my fellow students Fabienne Freiburghaus, Jonas Knüsel, Lukas Meyer, Roland Spaeti, and Cyril Topfel for many discussions.

... my parents for their support.

List of Figures

List of Tables

Bibliography

[1] Perkins, Donald H. "Introduction to High Energy Physics" (2000) 4^{th} edition, Cambridge University Press, Cambridge

[2] Mössbauer, Rudolf L. "History of Neutrino Physics: Pauli's Letters" `http://users.physik.tu-muenchen.de/sfb375/Server/ringberg_1997/mossbauer.ps.gz` (2007/04/11)

[3] Reines, F., and Cowan, C.L., Jr. (1959) Phys. Rev. **113**, 273

[4] Bilenky, S.M. "Bruno Pontecorvo: Mister Neutrino" (2006) arXiv:physics/0603039v3

[5] Danby, G. *et al.* (1962) Phys. Rev. Lett. **9**, 36

[6] `http://nobelprize.org`

[7] Bahcall, John N. (1964) Phys. Rev. Lett. **12**, 300-302

[8] Davis, Raymond Jr. (1964) Phys. Rev. Lett. **12**, 303-305

[9] Davis, Raymond Jr. *et al.* (1968) Phys. Rev. Lett. **20**, 1205-1209

[10] Hasert, F.J. *et al.* (1973) Phys. Lett. B **46**, 138-140
Hasert, F.J. *et al.* (1974) Nucl. Phys. B **73**, 1-22

[11] Benvenuti, A. *et al.* (1973) Phys. Rev. Lett. **32**, 800-803

[12] Perl, M.L. *et al.* (1975) Phys. Rev. Lett. **35**, 1489-1492

[13] Perl, M.L. *et al.* (1976) Phys. Lett. B **63**, 466-470

[14] Perl, M.L. *et al.* (1977) Phys. Lett. B **70**, 487-490

[15] Hirata, K. *et al.* (1987) Phys. Rev. Lett. **58**, 1490-1493

[16] Barnett, R.M. *et al.* "The Number of Light Neutrino Types from Collider Experiments" (1996) Physical Review D **54**, 1

[17] Kodama, K. *et al.* (2001) Phys. Lett. B **504**, 218-224 (arXiv: hep-ex/0012035v1, (2000))

[18] Hirata, K. *et al.* (1991) Phys. Lett. B **280**, 146-152

[19] Hirata (1994) Phys. Lett. B **335**, 237-245

[20] Abdurashitov, J.N. *et al.* (2000) Physics of Atomic Nuclei, Vol. 63, No. 6

[21] The Super-Kamiokande collaboration "Statement: evidence for massive neutrinos found" `http://www.ps.uci.edu/~superk/announce.html` (2007/05/21)

[22] Yao, W.-M. *et al.* (Particle Data Group) "Neutrino Properties" (2006) J. Phys. G **33**,1 and 2007 partial update for edition 2008 (`http:/pdg.lbl.gov`)

[23] Particle Data Group (July 2006) Particle Physics Booklet

[24] Mohapatra, R.N. and Pal, P.B. "Massive Neutrinos in Physics and Astrophysics" (1991) World Scientific Lecture Notes in Physics, Vol. 41

[25] Slansky, R. *et al.* "The Oscillating Neutrino - An Introduction to Neutrino Masses and Mixing" (1997) Los Alamos Science, Number 25

[26] Boehm, F. and Vogel, P. "Physics of Massive Neutrinos" (1992) 2^{nd} edition, Cambridge University Press, Cambridge

[27] Wu, C.S. *et al.* (1957) Phys. Rev. **105**, 1413

[28] Pretzl, K. "Einführung in die Elementarteilchenphysik" (2005) Vorlesung Sommersemester 2005, Universität Bern (unpublished)

[29] SLAC "Time Reversal Invariance" `http://www2.slac.stanford.edu/VVC/theory/timereversal.html` (2007/08/24)

[30] Yao, W.-M. *et al.* "Neutrino Mass, Mixing, and Flavour Change" (2006) Journal of Physics G **33**, 1 available on `http://pdg.lbl.gov/`

[31] Strumia, A. and Vissani, F. "Neutrino masses and mixings and ..." (2006) arXiv:hep-ph/0606054v1

[32] Wikipedia "Neutrino" `http://en.wikipedia.org/wiki/Neutrino` (2007/10/09)

[33] `www.jb.man.ac.uk/~smao/starHtml/nuclearFusion.pdf` (2007/10/09)

[34] Fukuda, Y. *et al.* (1998) Phys. Rev. Lett. **81**, 1562-1567

[35] Abe, K. *et al.* "A Measurement of Atmospheric Neutrino Flux Consistent with Tau Neutrino Appearance" (2006) Phys. Rev. Lett. **97**, 171801

[36] McKeown, R.D. and Vogel, P. (The Super-Kamiokande Collaboration) "Neutrino Masses and Oscillations: Triumphs and Challenges" (2004) arXiv:hep-ph/0402025v1

[37] Murayama, H. "Oscillation Parameter Plots" `http://hitoshi.berkeley.edu/neutrino` (2007/10/06)

[38] Mohapatra, R.N. *et al.* "Theory of Neutrinos" (2004) arXiv:hep-ph/0412099v2

[39] Wikipedia "Neutrino oscillation" `http://en.wikipedia.org/wiki/Neutrino_oscillation` (2007/10/07)

[40] OPERA collaboration "Opera Technical Design Report: DRAFT 2.0" (2004) (unpublished)

[41] CERN, INFN "The CERN Neutrino Beam to Gran Sasso - conceptual technical design", CERN 98-02, INFN/AE-98/05, 19 May 1998

[42] CNGS website `http://proj-cngs.web.cern.ch/proj-cngs` (2007/11/17)

[43] Autiero, D. "The OPERA event generator and the data tuning of nuclear reinteractions" (2004) presentation NUINT04 20/03/2004, LNGS

[44] Acquafredda, R. *et al.* (2006) New Journal of Physics **8**, 303

[45] Guler, M. *et al.* "OPERA Experiment Proposal" (2000) CERN/SPSC 2000-028

[46] Di Giovanni, A. "The VETO system of the OPERA experiment" (2005) presentation 10-12 October 2005, Seoul

[47] Bertolin, A. and Di Giovanni, A. "First results on the VETO commissioning" OPERA note 07-85

[48] Campagne, J.E. (2004) Eur Phys J C **33**, s01, 837-839

[49] Campagne, J.E. "Muon tracking in heterogeneous structures" October 4, 1999

[50] Agostinelli, S. *et al.* (2003) NIM A **506**, 250-303

[51] D'Agostini, G. "A Multidimensional Unfolding Method Based on Bayes' Theorem" (1994) DESY 94-099, ISSN 0418-9833